iScience

CellPress
OPEN ACCESS

Article

Lineage tracing reveals transient phenotypic adaptation of tubular cells during acute kidney injury

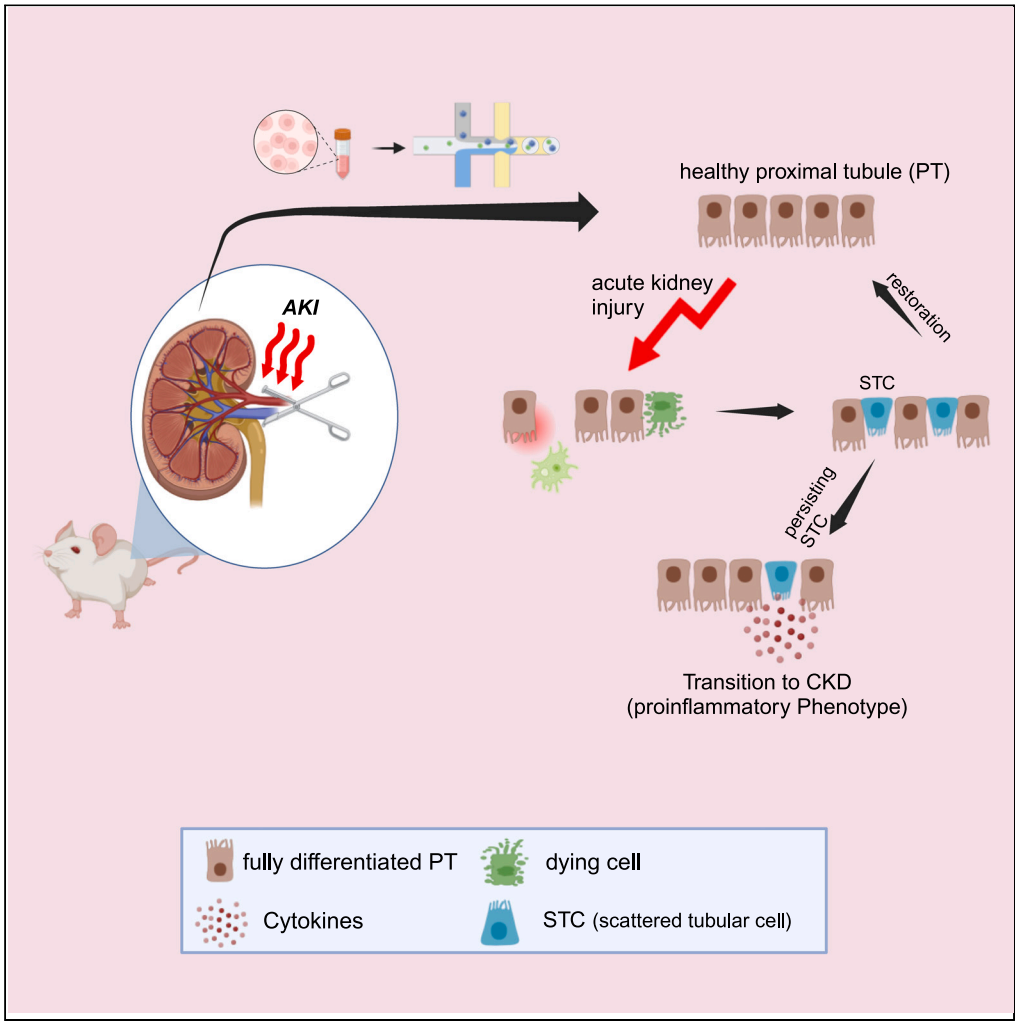

Marc Buse, Mingbo Cheng, Vera Jankowski, ..., Marcus J. Moeller, Ivan G. Costa, Eleni Stamellou

stamellou.eleni@gmail.com

Highlights

The PEC-rtTA marks specifically a regenerative cell type (STC) emerging after AKI

Lineage tracing revealed that STCs differentiate back into mature tubular cells

Prolonged activation of the STC phenotype leads to a proinflammatory behavior

STCs display a heterogeneous cell population

Buse et al., iScience 27, 109255
March 15, 2024
https://doi.org/10.1016/j.isci.2024.109255

iScience

CellPress
OPEN ACCESS

Article

Lineage tracing reveals transient phenotypic adaptation of tubular cells during acute kidney injury

Marc Buse,[1,9] Mingbo Cheng,[2,9] Vera Jankowski,[3,9] Michaela Lellig,[3] Viktor Sterzer,[1] Thiago Strieder,[1] Katja Leuchtle,[1] Ina V. Martin,[1] Claudia Seikrit,[1] Paul Brinkkoettter,[4] Giuliano Crispatzu,[4] Jürgen Floege,[1] Peter Boor,[1,5] Timotheus Speer,[6] Rafael Kramann,[1,7,8] Tammo Ostendorf,[1] Marcus J. Moeller,[1] Ivan G. Costa,[2] and Eleni Stamellou[1,10,*]

SUMMARY

Tubular injury is the hallmark of acute kidney injury (AKI) with a tremendous impact on patients and healthcare systems. During injury, any differentiated proximal tubular cell (PT) may transition into a specific injured phenotype, so-called "scattered tubular cell" (STC)-phenotype. To understand the fate of this specific phenotype, we generated transgenic mice allowing inducible, reversible, and irreversible tagging of these cells in a murine AKI model, the unilateral ischemia-reperfusion injury (IRI). For lineage tracing, we analyzed the kidneys using single-cell profiling during disease development at various time points. Labeled cells, which we defined by established endogenous markers, already appeared 8 h after injury and showed a distinct expression set of genes. We show that STCs re-differentiate back into fully differentiated PTs upon the resolution of the injury. In summary, we show the dynamics of the phenotypic transition of PTs during injury, revealing a reversible transcriptional program as an adaptive response during disease.

INTRODUCTION

Acute kidney injury (AKI) is a major clinical problem associated with significantly prolonged hospitalization, increased mortality, and higher healthcare costs.[1,2] Furthermore, AKI increases the risk of developing chronic kidney disease (CKD) or worsening underlying CKD.

Acute tubular epithelial cell injury is a common underlying pathological process of AKI and is most often due to ischemia, nephrotoxic injury, or a combination of both. Opposed to other epithelia, i.e., skin or intestine, which possess stem-cell populations responsible for continuous organ homeostasis, tubular cells are largely mitotically quiescent in healthy kidneys.[3–6] However, an intratubular subpopulation of proximal tubular epithelial cells emerges after AKI, proliferates and restores tubular integrity.[7–10] The origin of these cells has been a source of controversy. So far, two hypotheses exist: The first one argues for the existence of a stable intratubular progenitor/stem cell population.[11,12] The second hypothesis is based on the concept that any surviving tubular epithelial cell switch to a common injury response program, named scattered tubular cells (STCs). STCs express *de novo* marker proteins (e.g., CD44, kidney injury molecule (KIM)-1), show increased resistance to injurious stimuli and have a higher proliferative index.[13,14] We have previously demonstrated that the doxycycline-inducible parietal epithelial cell (PEC)-specific reverse-tetracycline transactivator (PEC-rtTA) transgenic mouse line labels with very high efficiency not only parietal epithelial cells (PECs) but also STCs.[13]

Increasing evidence supports the bidirectional link between AKI and CKD. Tubular epithelial cell damage, endothelial dysfunction, and interstitial inflammation are key factors in maladaptive repair and hence the AKI-to-CKD transition.[15–18] However, the exact mechanisms remain elusive. Previous studies employing a single-cell approach to investigate AKI identified a novel subpopulation of maladaptive cells after AKI. These cells were associated with the development of CKD, ascribed to their proinflammatory profile, and hypothesized to be incapable of regeneration.

[1]Division of Nephrology and Clinical Immunology, RWTH Aachen University, Aachen, Germany
[2]Institute for Computational Genomics, RWTH Aachen University Hospital, Aachen, Germany
[3]Institute for Molecular Cardiovascular Research, RWTH Aachen University Hospital, Aachen, Germany
[4]Department II of Internal Medicine and Centre for Molecular Medicine, University of Cologne, Faculty of Medicine and University Hospital Cologne, Cologne, Germany
[5]Institute of Pathology, University Hospital RWTH Aachen, Aachen, Germany
[6]Medical Clinic 4, Nephrology, University of Frankfurt und Goethe-University Frankfurt, Frankfurt am Main, Germany
[7]Institute of Experimental Medicine and Systems Biology, RWTH Aachen University, Aachen, Germany
[8]Department of Internal Medicine, Nephrology and Transplantation, Erasmus Medical Center, Rotterdam, the Netherlands
[9]These authors contributing equally
[10]Lead contact
*Correspondence: stamellou.eleni@gmail.com
https://doi.org/10.1016/j.isci.2024.109255

Single-cell mRNA sequencing (scRNA-seq) provides an unbiased tool to characterize transcriptional profiles associated with kidney injury and repair. In this study, we employed genetic fate-tracing experiments using labeling strategies to specifically study regenerating proximal tubular cells (PTs) in an unilateral ischemia-reperfusion injury (IRI) model using scRNA-seq. Our study provides gene expression patterns in STCs upon injury and repair at multiple time points and suggests that the STC phenotype is a transient and reversible phenotype triggered by injury.

RESULTS

Single-cell analysis after ischemia-reperfusion injury

AKI was induced in male quadruple-transgenic PEC-rtTA mice (9 weeks of age) by unilateral ischemia-reperfusion injury (IRI). Doxycycline was administered immediately after the induction of the injury to label emerging STCs for about 48 h (Figure 1A). $CD13^+$ cells (presumptive PTs) were isolated using fluorescence-activated cell sorting (FACS) for $CD13^+$/DAPI- (living) cells with subsequent 3′ scRNA-seq using the 10x Genomics pipeline. To rule out any influence of the sorting process on the examined cell population, we investigated the expression of CD13 in immunofluorescence over the course of injury. No significant decrease in the surface marker CD13 was observed after AKI compared to the controls (Figure S1E). Serum creatinine values were significantly upregulated 8 h after IRI (Figure 1B, upper graph). Histological analysis of kidney sections revealed significant tubular damage not present in the control group and confirmed AKI (Figure 1B, lower graph). Additionally, we quantified the expression of Kidney Injury Molecule-1 (KIM-1; coded by the gene *Havcr1*), a well-known marker of injury, using immunofluorescence. We observed a highly significant increase after AKI, providing further evidence for the effectiveness of our AKI model.

Next, we integrated time points and samples from healthy and injured kidneys followed by clustering analysis, which grouped cells into 17 separate clusters (Figure S1A and Data S1). In our analysis, we could define unique marker genes for all clusters in the integrated datasets and defined the relative abundance of each cluster in healthy versus injured kidneys. As expected, our datasets are strongly enriched for PTs in all experimental conditions. However, small non-PT clusters emerged after the injury. These non-PT clusters, consisting of monocytes and macrophages, appeared predominantly in the injured kidneys (Datas S2 and S3). They were not present in the controls or uninjured kidneys, indicating the lenient selection of $CD13^+$ cells during FACS sorting.

To corroborate our results, we selected the known injury marker gene *Havcr1* (coding for the protein kidney-injury-molecule-1), and several PT-marker genes such as *Ass1* and plotted their expression over time (Figure 1C). *Havcr1* was highly upregulated 24 h after unilateral IRI and decreased after 48 h. *Ass1* was markedly downregulated upon injury, but expression recovered over time and upon injury resolution (Figure 1C, lower graph).

For the in-depth characterization of the different PTs, we performed a re-clustering analysis of all PTs, excluding non-epithelial cells. After quality control filtering and re-clustering, we obtained 40,442 cells from mouse kidneys, yielding 11 clusters (Figures 1D and S1A). Clusters expressing *Havcr1* were identified as injured PTs and clusters expressing differentiated PT markers and not expressing *Havcr1* were defined as differentiated PTs. Based on the study by Kirita et al.,[19] differentiated PTs were further subdivided into distinct tubule segments, i.e., S1 (*Slc5a2, Slc5a12, Gatm, Asl*), S2 (*Slc7a13, Cyp4b1, Cesf1, and Slc34a1*) and S3 (*Slc7a13, Napsa, Cd36, Slac5a8, Slc27a2*) (Figure 1E and Data S3).

Parietal epithelial cell-specific reverse-tetracycline transactivator transgene becomes transcriptionally active immediately after tubular cell injury

The PEC-rtTA/LC1/R26R/H2BeGFP quadruple transgenic mouse expresses β-galactosidase irreversibly upon Cre recombination induced by transient the administration of doxycycline (Figure 2A, left side). In addition, the nuclei are loaded metabolically with histone coupled to an enhanced green fluorescent protein (H2BeGFP) during the administration of doxycycline (Figure 2A, right side). Further details can be found in the STAR Methods section under Lineage tracing. In our experimental setting, doxycycline was administered once directly after injury to label tubular epithelial cell transitioning into the STC phenotype. Based on our experience, H2B-eGFP labeling of STCs is estimated to continue for approximately 48–62 h.

AKI caused an elevated *H2B-eGFP* expression compared with the controls, as shown in Figure 2B. Eight hours after AKI, two new *H2B-eGFP*+ clusters were detected, which we annotated as "STC-S1" and "STC-S2/S3," as they displayed unique gene signatures of the proximal tubule segment S1 and -S2/S3 together with STC markers (Figure 2B, right graph; Figure S1D, Heatmap). As *H2B-eGFP* was also slightly present in normal PT clusters, we compared the expression profile of *H2B-eGFP*+ cells with the *H2B-eGFP*- cells in STC- and normal PT clusters (Figure S1B). Indeed, *H2B-eGFP*+ cells differed from *H2B-eGFP*- cells in STC clusters, showing the specific STC gene expression signature and hence indicating that the PEC-rtTAmouse specifically labels STCs. These clusters co-expressed the tubule injury marker-gene *Havcr1*, indicating that the *H2B-eGFP*+ cells (presumptive STCs) were "injured" PTs (Figures 2C and S1D, Heatmap). STC-S1 and STC-S2/S3 clusters arose 8 h after injury, increased until 24 h, and had already started to decrease by 48 h (Figures 2D and S1C). *H2B-eGFP* expression during injury followed the same pattern as *Havcr1* (Figures 2C and S1D). Co-expression of Kidney-injury-molecule-1 (KIM-1; coded by *Havcr1*) with H2BeGFP could be validated by immunofluorescence staining (Figure S2A). Interestingly, these clusters were similar to the injured S1/S2 and injured S3 generated by the Kim1CreER mouse, as described by Kirita et al.[19]

STC-S1 and STC-S2/S3 expressed a distinct set of genes. Some of the highly up-regulated genes are known markers of STC, such as *Havcr1*, *AnnexinA2*, *AnnexinA3*, *S100a6*, and *Spp1* (coding for the protein Osteopontin). Furthermore, a number of new marker genes could be identified. These included *Krt8/18, Lgals3* (coding for the protein Galectin-3), *Sfn, Cryab* (Figure 2E), and *Rbp4, Krt20* (not shown). *Cryab* encodes an alpha-crystallin B chain protein that is a part of the small heat shock protein family and functions as a molecular chaperone that primarily binds unfolded proteins to prevent protein aggregation and has been described to be cytoprotective against cisplatin

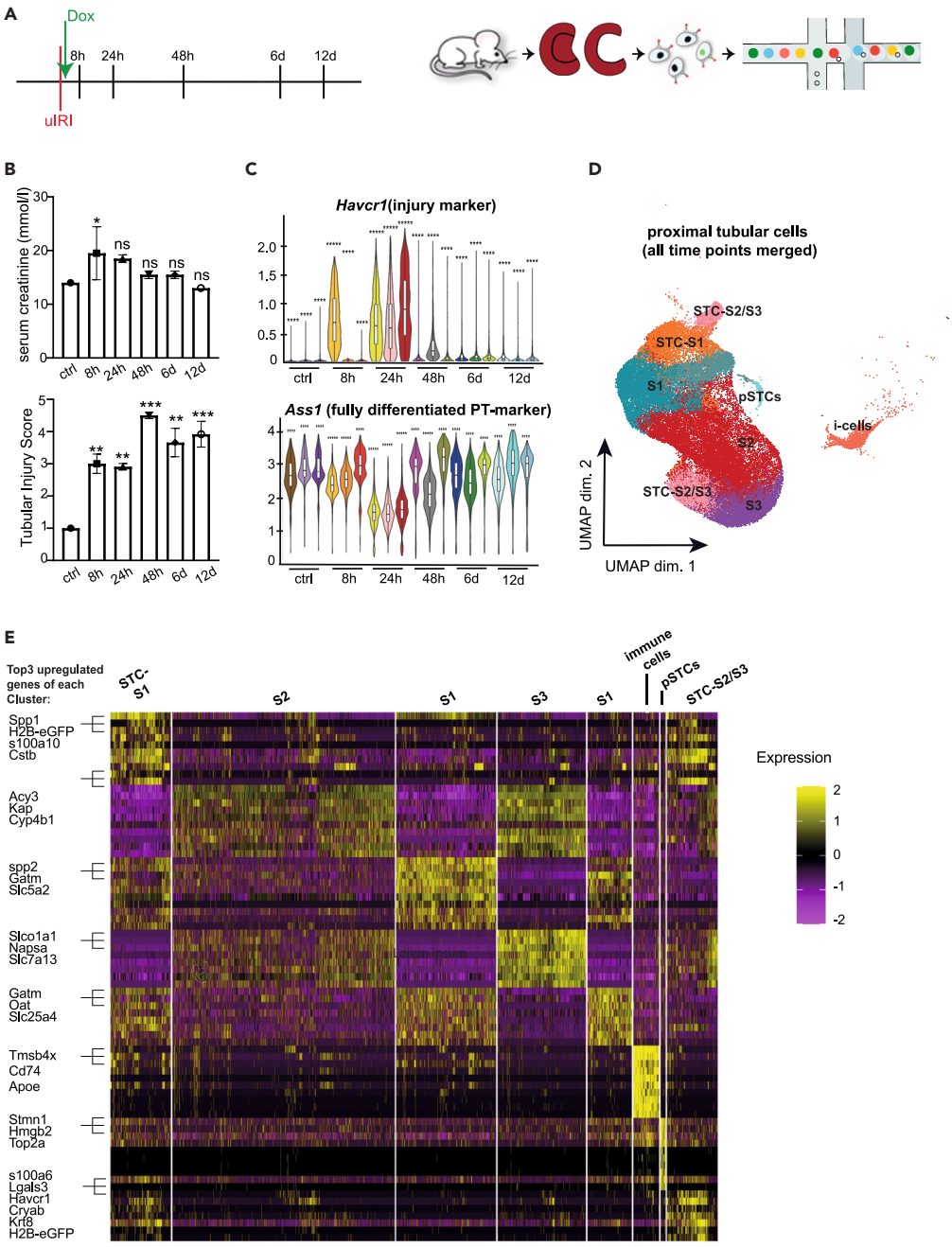

Figure 1. Single-cell RNA seq for CD13^{+} cells in the time course of IRI

(A) Scheme of experimental setting, n = 3 mice per group.

(B) Upper graph: creatinine (mmol/L) after sham (ctrl) and IRI. Data are shown as mean ± SD, lower graph: Tubular injury score in sham (ctrl) and IRI kidneys. Data are expressed as mean ± SD, ns p> 0.05, * p< 0.05, ** p< 0.01, *** p<0.001.

(C) Violin plots of *Ass1* and *Havcr1* expression in control and IRI mice. Every timepoint (controls and 8 h, 24 h, 48 h, 6 days, and 12 days after AKI) consists out of 3 samples (displayed in the different colors).

(D) UMAP plots of PTs in control and IRI mice integrated with Seurat. S1; S1 segment of proximal tubule, S2: S2 segment of proximal tubule, S3; S3 segment of proximal tubule, STC, scattered tubular cell, pSTC, proliferating scattered tubular cells, immune cells (i-cells); see also Figure S1A.

(E) Heatmap gene expression depicting the top three genes in each cluster.

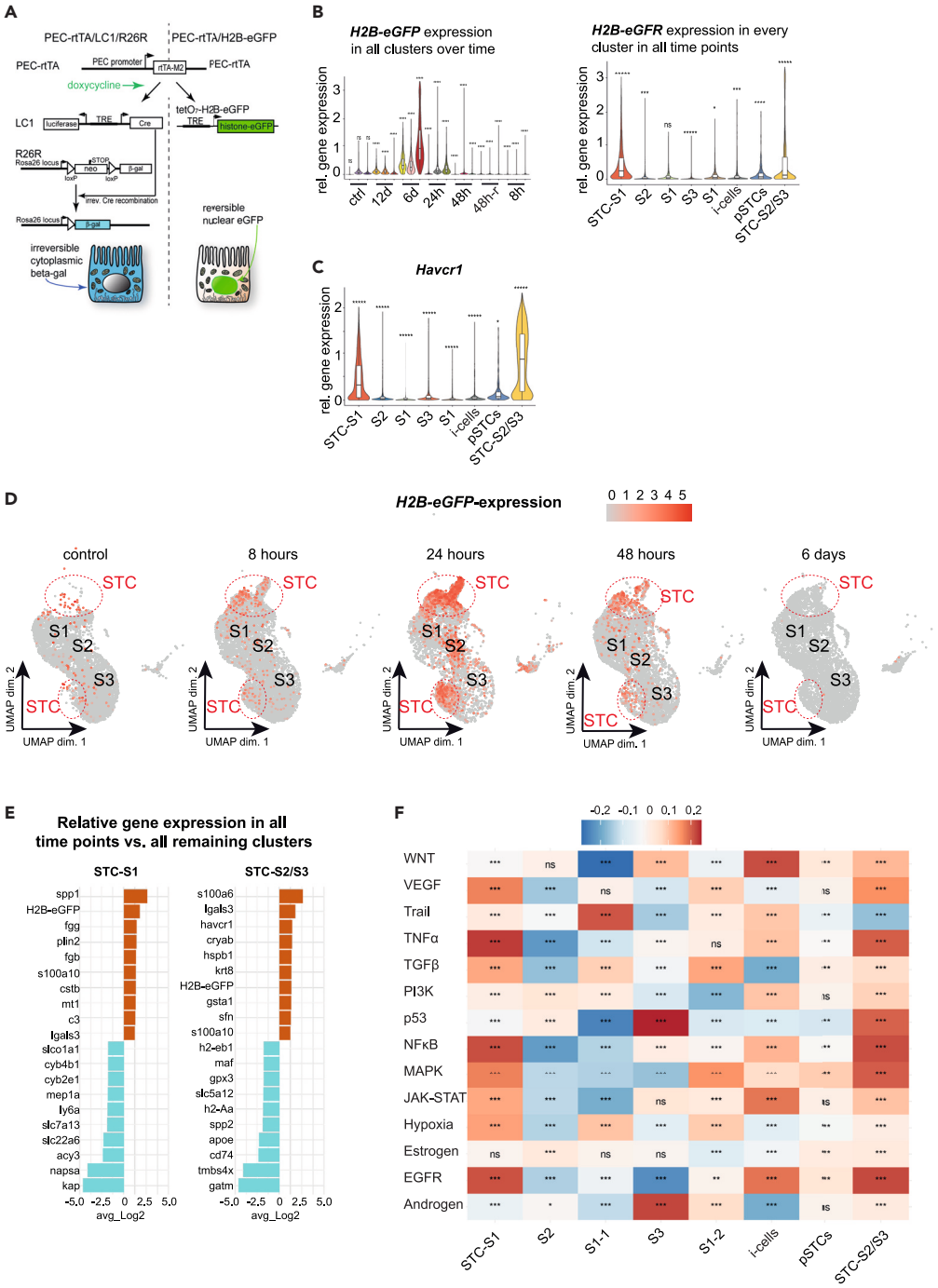

Figure 2. Scattered tubular cells

(A) Transgenic map of the 4x transgenic PEC-rtTA mouse. Three transgenic mRNAs are important: rtTA-M2 is expressed in PTs that are currently in the STC phenotype. *H2B-eGFP* will be expressed at very high levels in STCs only in a dox-inducible fashion. *LacZ* will be expressed constitutively in STCs after the administration of dox. When the cell reverts to the normal PT phenotype, it continues to constitutively express *LacZ*.

(B) Violin plot of the gene expression of *H2B-eGFP* over time (left graph; every timepoint consists out of 3 samples (displayed in different colors)) and across the different clusters (right graph, all timepoints merged). ns p> 0.05, * p< 0.05, ** p< 0.01, *** p<0.001. 48-r: right contralateral kidney, not injured; see also Figure S1D.

Figure 2. *Continued*

(C) Violin plot of the gene expression of havcr1 in the different clusters (all timepoints merged), * p< 0.05, **** p<0.0001. S1; S1 segment of proximal tubule, S2; S2 segment of proximal tubule, S3; S3 segment of proximal tubule, STC; scattered tubular cell, i-cells; immune cells, see also Figure S1D.

(D) UMAP plots of H2B-eGFP expression at different time points. S1; S1 segment of proximal tubule, S2; S2 segment of proximal tubule, S3; S3 segment of proximal tubule, STC; scattered tubular cell; see also Figure S2C.

(E) DE & GO expression of the top up-regulated and down-regulated genes in STC-S1 and STC- S2/S3.

(F) PROGENy pathway analysis of PTs. ns p> 0.05, * p< 0.05, ** p< 0.01, *** p<0.001, **** p<0.0001.

nephrotoxicity.[20] Keratins, the intermediate filaments of the epithelia cell cytoskeleton, are upregulated in cellular stress/injury.[21] In healthy mice, *Krt8/18* are expressed in the collecting ducts and glomerular epithelial parietal cells. It has been shown that their expression increases upon renal tubular injury.[22] *Krt20* (coding for the protein Keratin20) has been described as a *de novo* tubular injury marker and recently the role of Krt20+ cells in IRI was investigated.[23] *Lgals3* encodes Galectin 3 protein, a member of the lectin protein family, implicated in nephrogenesis and kidney disease, regulating cell growth and differentiation.[24,25] Interestingly, Sox9, a transcription factor associated with the repair of proximal tubules was expressed only in STC-S2/S3 and not in STC-S1 (Data S3), whereas at the protein level it appeared at later time points (6 and 12 days after injury) and co-localized with H2BeGFP (Figure S2C, left side).

The PROGENy pathway analysis suggested the enrichment of terms related to TNFα, p53, NF-κB, MAPK, VEGF, WNT, and EGFR (Figure 2F). Upregulation occurred particularly in S3 segments, which are more susceptible to ischemia.

Next, we examined the signaling pathways being upregulated in STCs across the different time points. By 8 h and for at least 48 h after injury, pathways related to Rho GTPases and GTPases effectors increased. Rho family small GTPases are known to regulate cell shape, migration and adhesion but also activate a number of signal transduction pathways involved in cell cycle progression, gene expression, and cell survival[26] (Figure S3A). On the contrary, pathways related to metabolism and synthesis were downregulated in all clusters but more predominantly in STCs (Figure S3B). By 48 h, proliferating STCs showed an increase in pathways related to SUMOylation and proliferation (Figure S3C). In STCs, pathways related to semaphorins and insulin growth factor were upregulated by 6 days after injury (Figure S3D). Interestingly, at 12 days after IRI, cell cycle and proliferation markers were found to be activated only in STCs-S1/S2 (Figure S3E).

Next, we performed a re-clustering analysis of STCs, and three distinct subpopulations were revealed. The first one (STC-A) was more similar to normal PTs and was also present in normal non-injured kidneys. The other two subpopulations increased 8 h after injury and decreased upon the resolution of the injury. Cluster STC-C expressed known STC marker-genes i.e., *H2B-eGFP*, *Krt8/18*, *Vimentin*, and *Akap12*, while cluster STC-B demonstrated a more inflammatory phenotype expressing *Havcr1*, *Cxcl16*, *CD74*, and *MHC* molecule genes (Figure S4).

Immunofluorescence studies confirmed the up-regulation of the newly identified STC markers in H2B-eGFP + cells showing co-localization ranging between 25 and 50% (Figure 3A). Next we validated our findings in human biopsies from kidney transplant patients with acute kidney injury due to ischemia-reperfusion injury. By light microscopy, biopsies showed marked injury of tubular cells (data not shown). Given that CD24 is a known STC marker, we performed immunofluorescence staining and confocal staining of CD24 with STC markers. We investigated five human samples with acute tubular necrosis (ATN), and CD24 was markedly increased and co-localizated with STC-marker proteins S100a6, and S100a10 (Figure 3B), hence confirming that our mouse model labels STCs.

Proliferating scattered tubular cells

A high proliferating cluster arose 24 h after injury, grew up to 48 h and almost disappeared by day 12. As this cluster had enrichment of "cell cycle" genes, including the up-regulation of *Ki-67*, *Top-2a*, and *stmn1*, which are essential for proliferation (Figure 4A), we annotated this cluster as proliferating STC (pSTC). Cell cycle status analysis confirmed that this cluster had the highest proportion of cycling cells, followed by STC-S1 and STC-S2/S3 (Figure 4B). By 6 days, there was no evidence of pSTCs, hence confirming also previous reports.[19] Finally, these cells showed the highest *LacZ* expression among all clusters (Figures 4C and S1D, Heatmap).

Scattered tubular cells differentiate back to normal tubular cells

As transgenic eGFP coupled to histone B2 (H2B-eGFP+) labels STCs only reversibly, we analyzed the expression of transgenic *LacZ* (coding for β-galactosidase), which is activated in cells in the STC phenotype in an irreversible fashion. After this, these cells can be detected indefinitely even if they no longer exhibit the STC phenotype. As seen in Figure 5A, the numbers of *LacZ* expressing cells increased over time. The first increase occurred in STC clusters 24 h after AKI. At later points, *LacZ*-expressing PTs increased in differentiated PT clusters (Figures 5A and 5B), while *LacZ*+ cells were more similar to normal differentiated PTs and localized in the differentiated PT clusters. Induction of transgenic labeling no longer occurred after 48 h as shown in Figure 2D. Consequently, these findings suggest that STCs re-differentiate back to the normal fully differentiated PT phenotype.

Kirita et al. showed previously that PT subgroups (segments S1-3) can be differentiated into the STC phenotype.[19] This allows pseudotime trajectory and diffusion map analysis of the individual PT segments. As shown in Figure 5C, STCs potentially differentiate from STC phenotype back to fully differentiated individual PT subgroups taking three different directions; one directed to S1 tubule, one to S2 and the third toward S3 tubule. Individual gene expression changes were analyzed upon the re-differentiation of STCs to PTs based on the trajectory. Re-differentiation back into the PT phenotype was characterized by the up-regulation of PT-specific sub-segment-specific marker-genes (*Slc7a13, Slc5a2*) (Figure 5D) and down-regulation of STCs marker-genes (*Krt8/18* and *S100a6*) (Figure 5E). Down-regulation of STC markers was confirmed at the protein level using immunofluorescence staining (Figure 5E).

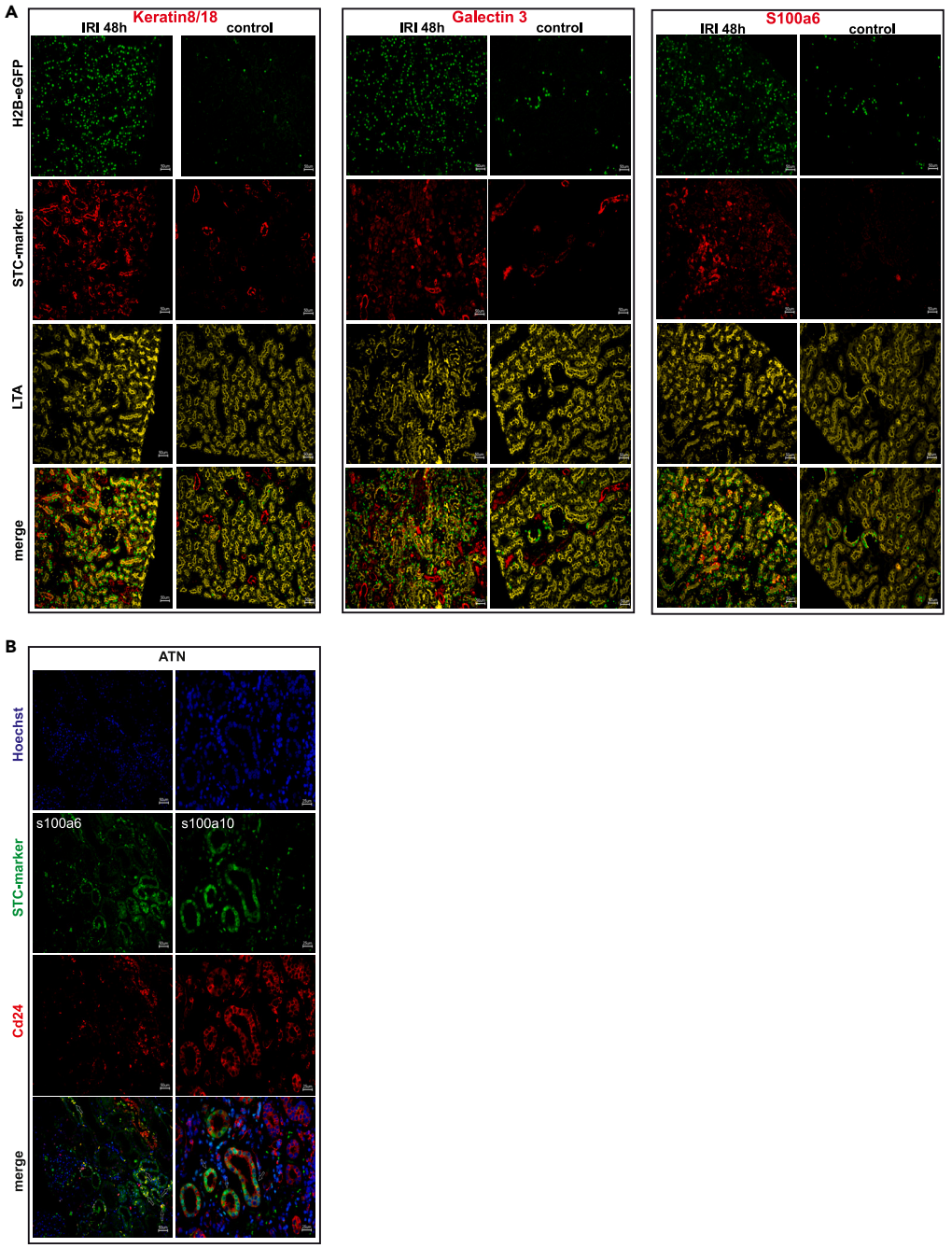

Figure 3. Characterization of STCs

(A) Representative images of immunofluorescence staining for H2B-eGFP (green), Keratin8/18 (corresponding gene: Krt8/18) (red), S100a6 (red), Galectin 3 (red), and Lotus Tetragonolobus Lectin (LTA; yellow) in control and IRI mice (evaluated in a 40× visual field in three experimental mice 48 h after injury).

(B) Representative images of immunofluorescence staining for Cd24 (green), S100a6 (red), s100a10 (red) in patients with acute tubular necrosis (ATN).

Scattered tubular cells 4 weeks after acute kidney injury

Immunohistochemical staining for collagen-3 revealed a significant onset of fibrosis as early as 12 days, indicating a maladaptive response to our AKI model (Figure S5E). Subsequently, we generated scRNA-seq data from $CD13^+$ cells in mouse kidneys 4 weeks after AKI. In contrast to the preceding experiments, doxycycline was administrated 24 h before analysis for this pulse labeling experiment (Figure 6A). After quality control filtering, we obtained 4058 cells (Figure S5A). $CD13^+$ cells were isolated using FACS with subsequent 3′scRNA-seq as above.

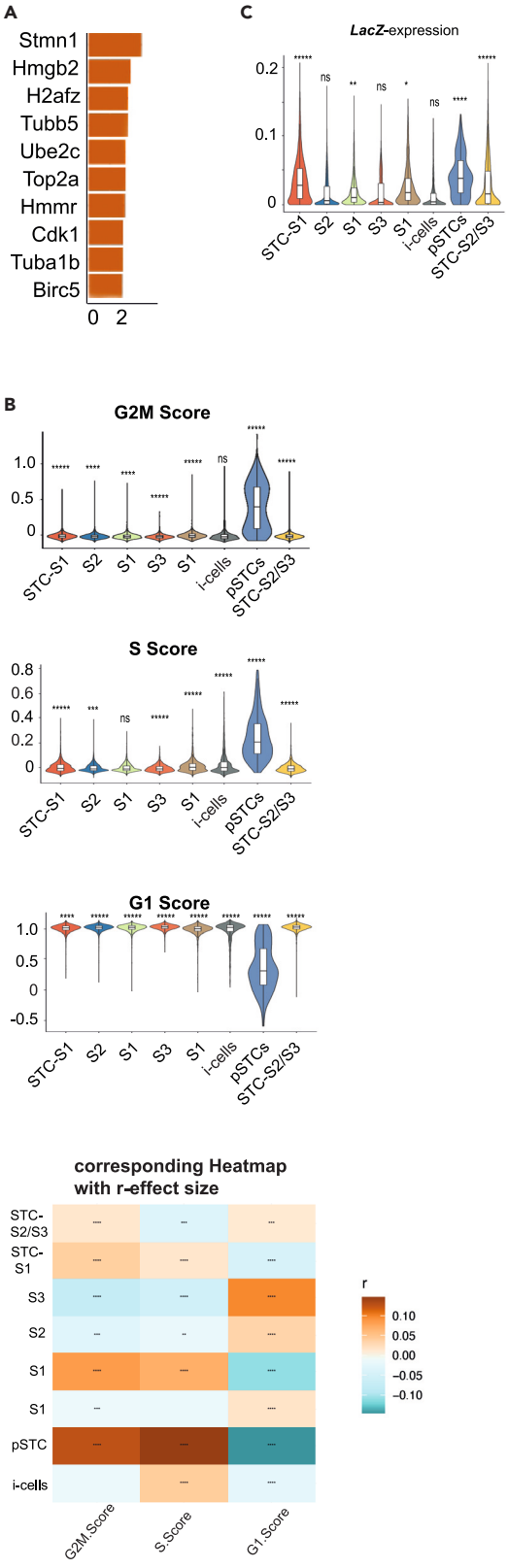
A
Stmn1
Hmgb2
H2afz
Tubb5
Ube2c
Top2a
Hmmr
Cdk1
Tuba1b
Birc5
0 2
C
LacZ-expression
0.2
0.1
0
STC-S1
S2
S1
S3
S1
i-cells
pSTCs
STC-S2/S3
B
G2M Score
S Score
G1 Score
corresponding Heatmap
with r-effect size
STC-S2/S3
STC-S1
S3
S2
S1
S1
pSTC
i-cells
G2M.Score
S.Score
G1.Score
r
0.10
0.05
0.00
−0.05
−0.10

Figure 4. Proliferating cells

(A) DE&GO gene expression of top 10 genes within the cluster of proliferating cells (pSTCs).

(B) Cell cycle analysis of each cluster (all timepoints merged). Violin plots showing the number of cells in each cluster in the different cell cycle phases; S, G2M, and G1. Corresponding Heatmap with r-effect size (all timepoints merged), ns $p > 0.05$, * $p < 0.05$, ** $p < 0.01$, *** $p<0.001$, **** $p<0.0001$.

(C) Violin plot of LacZ gene expression among the different PT clusters (all timepoints merged), ns $p > 0.05$, * $p < 0.05$, ** $p < 0.01$, *** $p<0.001$, **** $p<0.0001$. S1; S1 segment of proximal tubule, S2; S2 segment of the proximal tubule, S3; S3 segment of the proximal tubule, STC; scattered tubular cell, pSTC; proliferating scattered tubular cells.

Clustering analysis indicated 7 groups, as visualized in the UMAP space (Figure 6B). As expected, 4 weeks after injury our datasets were strongly enriched for fully differentiated PTs (Data S4). Expression analysis of the marker genes of the PEC-rtTA mouse showed enrichment predominantly in the very small STC-Cluster (Figure 6B). This cluster expressed *Cd24*, *Vimentin*, *Akap12*, *S100a6*, and *S100a10*, all known markers of STCs (Table 1). Cell cycle status analysis did not show any increased proliferation activity (Figure S5B). Reactome pathway analysis suggested *TGF-β* signaling activation (Figure 6C). Tubular injury marker genes such as *Krt8/18, Krt20* were not expressed in any of the cell clusters, except for *Havcr1*, which remained up-regulated in the S3 segment (Figure S5C). The S3 segment expressed genes associated with terminally differentiated PTs, while also showing the up-regulation of *Serpin* genes (Figure S5D, Data S4).

Scattered tubular cells in chronic kidney disease stage 2–3

To assess whether the STCs that did not redifferentiate into fully differentiated PTs contribute to the progression to CKD we investigated the association between four known STC marker proteins (Vimentin, Annexin A2, S100a10 and Keratin 7) and kidney function in a cohort of patients with CKD. We investigated plasma samples from 15 patients: 5 healthy controls, 5 with CKD stage 2, and 5 CKD stage 3 by using mass spectrometry (Table 2). As shown in Figure 6E, the intensity of circulating STC-markers increased significantly in patients with CKD with more advanced kidney dysfunction, i.e., with markedly reduced eGFR, which suggests the existence of STCs in the kidneys of patients with CKD.

DISCUSSION

In this study, following acute kidney injury, we characterized the fate of a specific fraction of proximal tubular cells, the scattered tubular cells (STCs), by performing inducible and reversible as well as irreversible tagging of these cells after unilateral ischemia-reperfusion (IRI) in PEC-rtTA mice.

The first major finding of our study was that in the course of acute kidney injury the induced STCs returned back to their normal fully differentiated phenotype. Cells in the STC phenotype occurred early after injury. Trajectory analyses, validated by immunostainings, showed that STC marker genes were downregulated by time, while the expression of genes encoding for proximal tubular transporters increased with the resolution of injury. Thus, this study provides the first evidence that injured PTs, that have transitioned to the STC phenotype after injury actually differentiate back into normal PTs after injury resolution. This establishes a specific and reversible transcriptional program (termed STC phenotype) that is activated upon injury in a unilayered epithelium. Our findings on the transient nature of STCs are thus consistent with previous data, showing that PTs develop a molecularly distinct pro-inflammatory and transient state (SOX9+VCAM1+ cell population) after mild injury and revert to their original state without inducing fibrosis.[27,28] These findings also contrast with those in other epithelia, i.e., skin, liver, or intestine which possess stem-cell populations responsible for continuous organ homeostasis.[3–6]

In addition, we were able to characterize STCs in more detail using single-cell sequencing. A number of new marker genes were identified, including *Krt8/18, Lgals3, Sfn1, Cryab, and Rbp4, Krt20*. It has been previously described that keratins are rapidly activated upon injury in epithelial cells in the proximal tubule and remain in degenerated proximal tubules after repair.[29] In addition, pathway analyses have highlighted several candidate pathways potentially involved in this phenotype switch. Migration, proliferation, and repair are the three crucial processes that injured tubular cells must undertake to complete structural and functional regeneration. Recent evidence suggests that interactions between integrins and extracellular matrix proteins promote the repair of injured PTs and that cell adhesion molecules are implicated in the control of cell mitogenesis, differentiation, anchorage dependence, and apoptosis.[29–32] Notably, we identified pathways related to cell communication, such as integrins, cell adhesion molecules (i.e., L1CAM), and RhoGTPases, to be up-regulated in STCs. Sox9 is a transcription factor associated with the repair of proximal tubules.[33,34] In an urothelial injury model, the induction of Sox9 was observed due to the activation of the epidermal growth factor receptor (EGFR) signaling pathway.[34] In our analysis, we have now observed activation of the EGFR signaling pathway in STCs early in the course of injury.

Next, our data suggest that STCs represent a heterogeneous cell population, as we isolated a subcluster with a markedly proinflammatory phenotype in addition to the already described STC phenotype. These STCs were characterized by the upregulation of MHC molecules, *Cd74*, complement components, and the downregulation of terminal differentiation markers. Expression of proinflammatory and profibrotic cytokines and myeloid cell chemotactic factors has been previously described in maladaptive/profibrotic PTs.[29,35]

Four weeks after injury, STCs were rare and accounted for only 0.4% of the PT population. These late STCs expressed the well-known STC marker-proteins Cd24, Vimentin, and S100a6, but not acute injury marker-genes such as *Havcr1* or *Krt8/18*. This suggests that these cells represent STCs that failed to re-differentiate after AKI. Interestingly, a similar PT population was also identified by Rudman-Melnick et al. In their study, a cell subpopulation with a mixed phenotype, termed "mixed-PT," was characterized by elevated protein expression of Sox4, Cd24, and Vimentin.[23] Similarly, Kirita et al. and Gerhardt et al. described a cell population, termed "failed-repair PTs" or "maladaptive PTs."[19,36,37] These cells appeared late in the course of injury and were characterized by the up-regulation of a new distinct set of genes such as

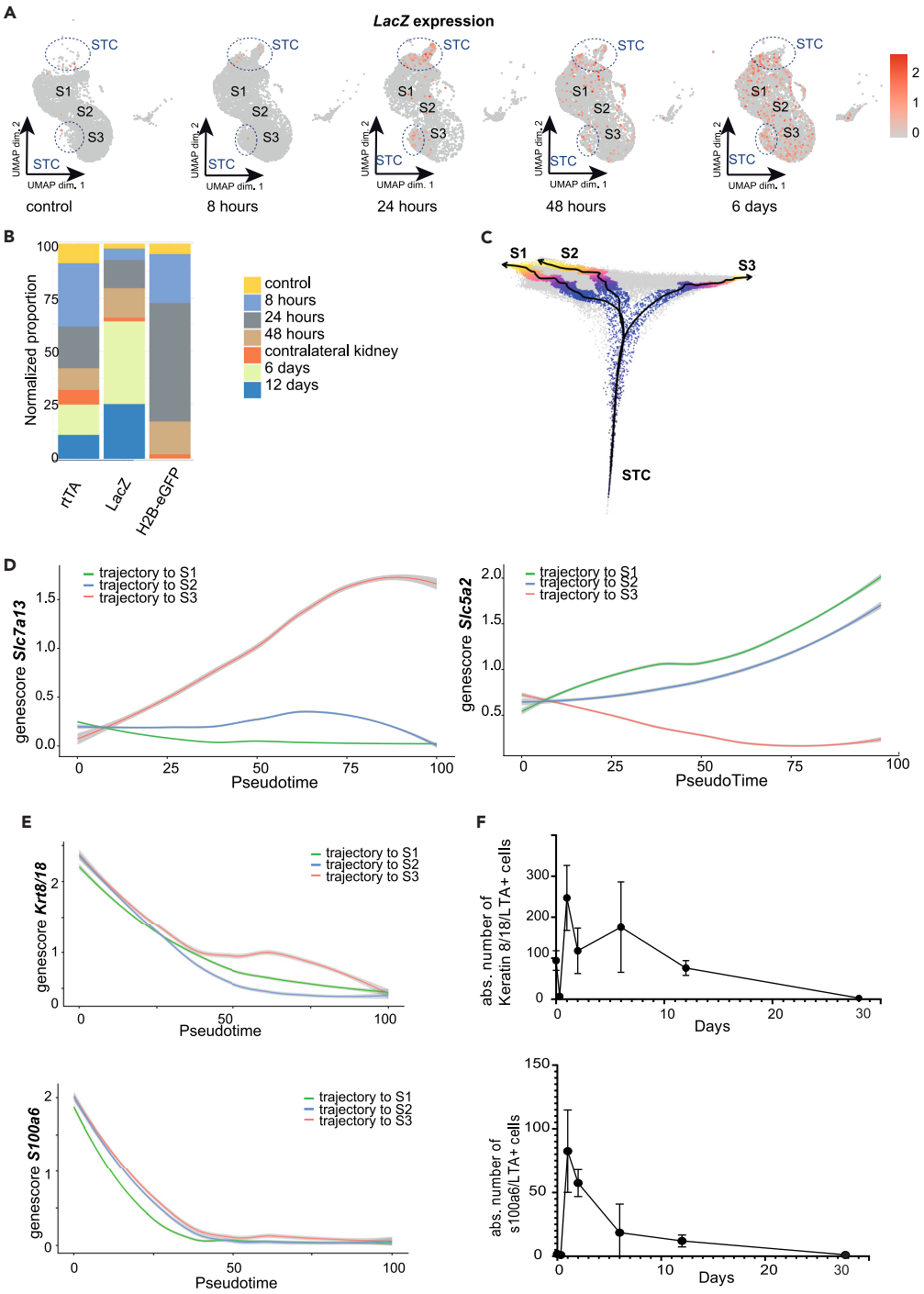

Figure 5. STCs differentiate back into normal PTs

(A) UMAP plots of LacZ expression at different time points. S1; S1 segment of proximal tubule, S2; S2 segment of proximal tubule, S3; S3 segment of proximal tubule, STC; scattered tubular cell.

(B) Proportion of *rtTA*- (Transactivator), *LacZ*- (corresponding Gene to B-Galactosidase), or *H2B-eGFP*-positive cells at each time point after AKI (C) Pseudotime trajectory of STC cells.

(D) Gene expression of *Slc7a13* and *Slc5a2* in pseudotime based on the trajectories.

(E) Gene expression of *Krt8/18* and *S100a6* in pseudotime, based on the trajectories. (F) Absolute numbers of Keratin8/18/LTA–and s100a6/LTA-expressing cells at different time points (evaluated in a 40× visual field in three experimental mice at six different time points after injury and control). Data are expressed as mean ± SD.

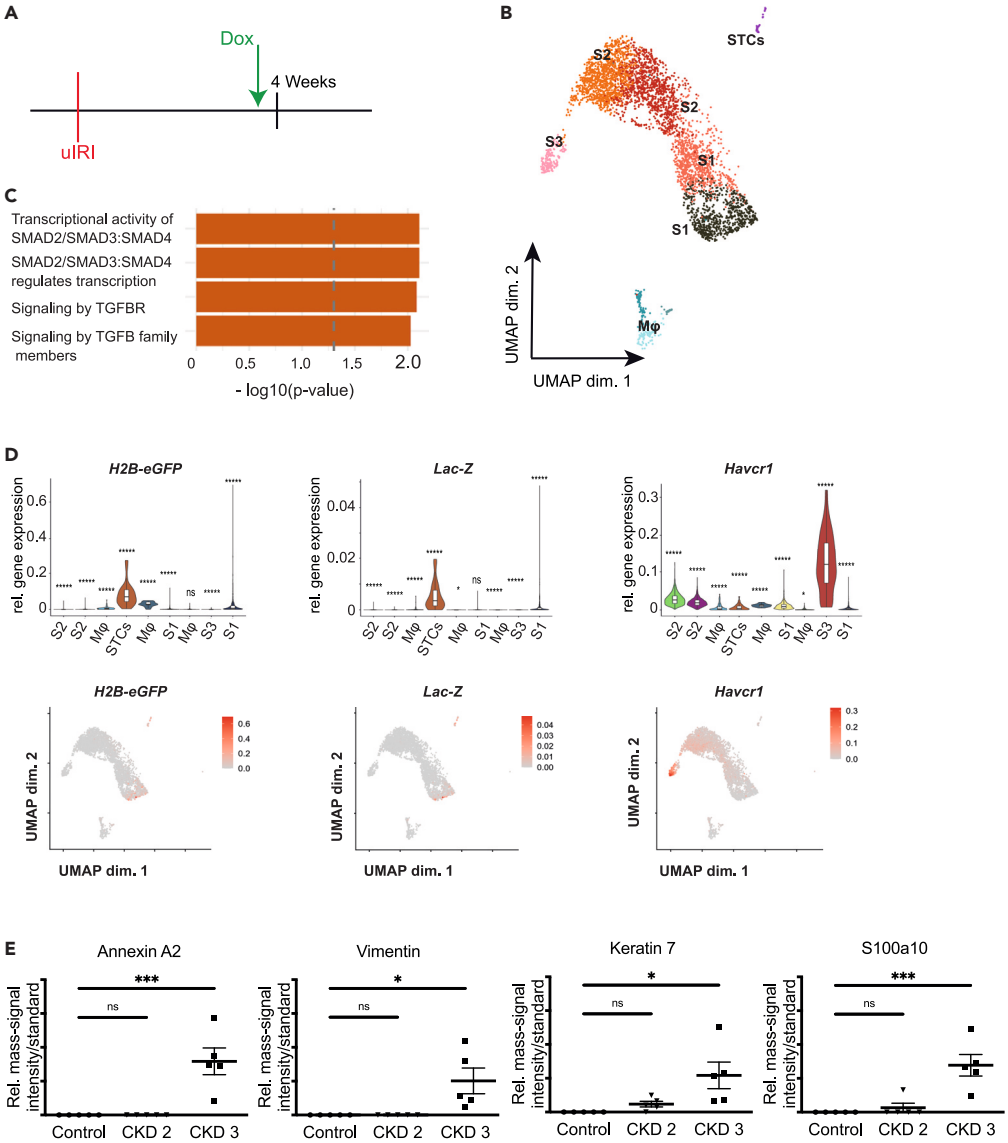

Figure 6. STCs 4 weeks after AKI

(A) Scheme of experimental setting.

(B) UMAP plots of IRI mice 4 weeks after injury integrated with Seurat. S; S1 segment of proximal tubule, S2; S2 segment of proximal tubule, S3; S3 segment of proximal tubule, STC, scattered tubular cell, macrophages (Mφ); see also Figure S5A.

(C) Reactome pathways analysis of IRI mice 4 weeks after injury.

(D) Violin plot and UMAP of *H2B-eGFP* and *LacZ* gene expression among the different PT clusters 4 weeks after AKI. S1; S1 segment of proximal tubule, S2; S2 segment of proximal tubule, S3; S3 segment of proximal tubule, STC; scattered tubular cell, Mφ, macrophages. Corresponding Heatmap with r-effect size in suppl. Figure 5C (right graph); see also Figure S5C (E) Plot of the relative intensity of the mass signal of Annexin A2, Vimentin, Keratin 7 and s100a10 in the serum of healthy human controls, and humans with CKD stage 2 and 3 (n = 5 per CKD-Stage; n = 5 in the Healthy controls-group; n = number of patients). Data are expressed as mean ± SD, ns p>0.05, *p< 0.05, **p<0.01, ***p<0.001, see also Table 2.

Vcam-1, *Ccl2, Pdgfd,* and down-regulation of terminal differentiation genes. They acquired a proinflammatory and profibrotic phenotype, and it has been suggested that they may be involved in the progression from AKI to CKD.[38,39] Moreover, Balzer et al.[35] identified a specific maladaptive/profibrotic PT cluster that expressed proinflammatory and profibrotic cytokines and was associated with the activation of inflammatory cell death pathways (pyroptosis and ferroptosis). In our STC transcriptomic data, we could identify genes that are associated with ferroptosis (e.g., *Chac1, Acsl4, Hmox1*),[40–42] particularly in the STC-S3 fraction (Data S3). Balzer et al. have recently proposed a so-called maladaptive repair cell state for cells that continuously express injury markers (e.g., *VCAM*).[35] Although we could not identify *Ccl2* or *Vcam* in our transcriptomic data, we could show in the immunofluorescence that STCs labeled in the PEC-rtTA mouse colocalize with Vcam-1 and Sox9

Table 1. Gene expression of STC markers in the STC-cluster, 4 weeks after AKI

Gene	log fold change[a]	% of cells where the gene is detected in the STC cluster	% of cells where the gene is detected in the rest of the clusters
cd24	2.06	0.48	0.003
egf	1.84	0.25	0.005
cryab	2.84	0.28	0.020
s100a6	1.69	0.19	0.014
vimentin	1.39	0.21	0.002
akap12	1.15	0.17	0.001

[a]log fold change of the gene expression between the STC cluster and the rest of the clusters.

(Figures S2B and S2C). To verify whether we lost VCAM+ cells during cell isolation due to reduced CD13 expression, we investigated the CD13 expression of VCAM+ cells using immunofluorescence and we could observe that these cells express CD13 (Figure S7). Presumably, this cell population is numerically very small and might be obscured in our transcriptomic data.

In another study, S. Kumar et al. demonstrated the significance of the transcription factor Sox9 during the regeneration process after AKI.[33] In their work, they showed that following AKI, surviving proximal tubular cells activate Sox9, and the absence of this transcription factor leads to impaired regeneration. Furthermore, they demonstrated that Sox9+ cells colocalize with KIM-1 and exhibit proliferative activity. The persistence of these Sox9+ cell populations was associated with fibrosis and progression to CKD. This described cell population aligns with the STCs we identified, as evident in both the transcriptome (*Havcr-1* colocalizing with *H2B-eGFP*) and the immunofluorescence (colocalization of Sox9+ and eGFP; Figure S2C) analyses.

Taken all together, our results are consistent with the literature in suggesting that our STCs resemble the previously unknown cell population which emerges after AKI.[23,33,43] Our investigations have shown that whether they are repair-failed PTs, poorly adapted PTs, Sox9+-cells or mixed PT fractions, they appear to be the same cell population at different stages of differentiation. We further suggest that the prolonged presence of STCs after the resolution of the injury is associated with fibrosis and the transition to CKD. In support of this, we found that the intensity of circulating STC markers is significantly increased in the sera of patients with CKD. Loss of tubular cell polarity, increased transepithelial permeability, and altered microvascular permeability are among the factors that facilitate the movement of tubular proteins into the circulation.[44–46]

In recent years, the influence of *Havcr1* (coding for KIM-1) on inflammation following AKI has been the subject of controversy. Humphreys et al. demonstrated a proinflammatory effect of chronic KIM-1 expression in a mouse line constitutively expressing KIM-1 since birth.[47] However, another study by the same group, however, revealed a protective effect of KIM-1 during the acute phase of AKI by reducing the NF-KB signaling pathway.[48] Our results align with the current literature. In our study, STC-S1 and STC-S2/S3 show increased Havcr-1 expression, indicating a protective effect, contributing to AKI regeneration, consistent with the protective effect of KIM-1 during the acute phase of AKI. Furthermore, we observed that some STC-S1 or STC-S2/S3 do not revert to a differentiated tubular cell after 4 weeks and maintain their phenotype. These cells display elevated Havcr-1 expression, as validated in immunofluorescence (Figure S2A (4 weeks)). Additionally, we detected elevated STC markers in the serum of patients with CKD. Existing literature suggests that higher KIM-1 levels in the plasma of patients with post-AKI contribute to CKD progression.[49] In summary, we believe that the short-term expression of KIM-1 may support the regeneration process, while long-term expression in the kidney leads to maladaptation and drives progression toward CKD. A novel insight here is that the persisting KIM-1-positive cells contributing to long-term maladaptation are likely STCs that have not reverted to a differentiated tubular cell state.

Next, our findings suggest that proliferating STCs originate from injured PTs. In agreement with data from the literature, these cells were observed 48 h after injury and disappeared after resolution (15). While they did not acquire the transcriptional phenotype described for STC-S1 and STC-S2/S3, they expressed *LacZ*, which is irreversibly expressed in STCs upon the administration of doxycycline. Notably, in our analysis, we did not observe the G2/M phase in STCs at 4 weeks after injury, and also Gerhardt et al. did not observe the G2/M phase in *VCAM1+* cells in their analyses on day 28 after IRI.[43] However, these findings cannot definitively exclude the possibility that these cells represent a progenitor population.

Table 2. Patients' baseline characteristics

	Healthy controls (n = 5)	CKD Stage 2 (n = 5)	CKD Stage 3 (n = 5)
Sex (male)	80%	60%	80%
Age	68.2 ± 6.6	56 ± 10.1	65 ± 11
Diabetes	20%	20%	40%
CVD	0%	0%	20%

CVD; cardiovascular disease.

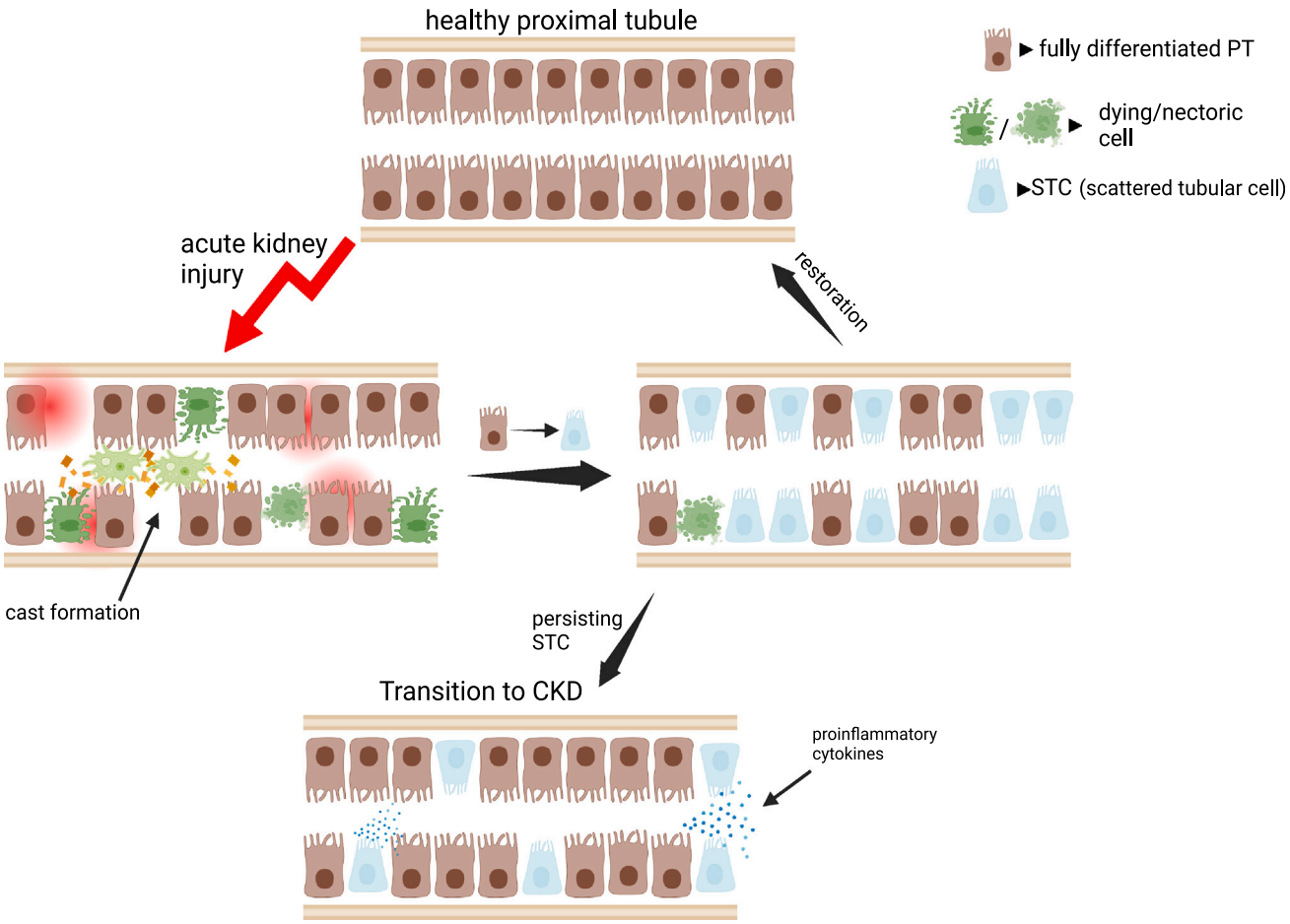

Figure 7. The figure illustrates the pathophysiological processes following AKI

After damage to the proximal tubule due to AKI (left in the figure), the surviving proximal tubular cells activate a regenerative program and transform into STCs (right in the figure). If the STCs manage to regenerate, they re-differentiate back into a fully mature proximal tubule cell and the former function could be restored. However, if regeneration fails, the STCs persist and fuel the development of maladaption and fibrosis, often marking the starting point of the transition to CKD (Chronic Kidney Disease; bottom); (Created with BioRender.com).

We found that 12 days after IRI cell cycle and proliferation markers were activated in STCs-S1/S2. Because the S1 segment is less susceptible to ischemia, this late proliferative signal could be a consequence of nephron loss with subsequent glomerular hyperfiltration and glomerular tubularization, which has been commonly observed after AKI.[50]

Our study has several limitations. First, it could be argued that by sorting $CD13^{+}$ cells, we may have excluded severely injured PTs from our analysis. However, our aim was to focus on the injured PTs that participate in the regeneration of the tubule. The phenotype of severely injured PTs has already been described.[19] However, we were also able to exclude through validation in immunofluorescence analysis that there is a significant decrease in CD13 after AKI (Figure S1E). Second, it could be argued that our mouse model randomly labels PTs and not specifically STCs, as evidenced by the presence of *H2B-eGFP+* cells in normal PT clusters. However, our hypothesis assumes that the STC phenotype is specific but also transient. This implies that PTs can be in the STC phenotype or in an intermediate state, correspondingly with more resemblance to fully differentiated PTs or to STCs. Hence, the existence of *H2B-eGFP+* cells in normal PT clusters can be explained by the transitional nature of the STC phenotype.

In conclusion, our study sheds new light on the role of STCs in kidney injury and repair. By analyzing gene expression patterns specific to STCs at multiple time points, we were able to show that the STC phenotype is a transient and reversible response to injury. Our results suggest that specific STC targeting could be a promising therapeutic strategy to enhance tubular regeneration and increase resistance to injury. In addition, we propose that the failure of STCs to re-differentiate into fully differentiated PTs may be associated with fibrosis development. Our investigations also provide new insights into the mechanisms underlying the progression from AKI to CKD. Overall, our study contributes to a better understanding of the dynamic nature of STCs in renal damage and repair (Figure 7). These findings could lead to the development of new therapeutic approaches for the prevention and treatment of AKI and CKD.

Limitations of the study

Our work does not provide insights into gender-specific differences. Previous studies have indicated that male mice exhibit greater sensitivity to ischemia-reperfusion.[51] For this reason, we used male mice, which are more susceptible to injury. Moreover, the samples for the mass spectrometric investigations also predominantly originate from male subjects, thereby limiting the generalizability to the female sex as well. In addition, in our study, 9-week-old healthy male mice were utilized. Consequently, it is questionable whether our observations would similarly reflect in multimorbid organisms with pre-existing health conditions. Ultimately, our results primarily rely on mouse data, and caution should be exercised when interpreting their direct applicability to other organisms, especially humans.

STAR★METHODS

Detailed methods are provided in the online version of this paper and include the following:

- KEY RESOURCES TABLE
- RESOURCE AVAILABILITY
  - Lead contact
  - Materials availability
  - Data and code availability
- EXPERIMENTAL MODEL AND STURDY PARTICIPANT DETAILS
  - Human-samples: Ethics statement
  - Animal studies - Mice
- METHOD DETAILS
  - Mouse kidney samples
  - Isolation of single cells
  - FACS
  - Tubular injury score
  - Light microscopy
  - Serum creatinine measurement
  - Immunofluorescence staining
  - CD13-quantification
  - Collagen-3-quantification
  - Immunhistochemistry
  - scRNA-seq data analysis
  - Mass spectrometry of serum proteins (MALDI MS)
  - Mass spectrometry of serum proteins (MALDI MS)
- QUANTIFICATION AND STATISTICAL ANALYSES

SUPPLEMENTAL INFORMATION

Supplemental information can be found online at https://doi.org/10.1016/j.isci.2024.109255.

ACKNOWLEDGMENTS

This research was supported by the STOP-FSGS consortium by the German Ministry for Science and Education (BMBF, STOP-FSGS-01GM2202C to MJM., ES, and PB), and by the Deutsche Forschungsgemeinschaft (DFG, German Research Foundation) Clinical Research Unit 5011, project number 445703531 (to RK, IC, ES, VJ, PB, TO, MM and JF). E.S. is supported by an START grant (19/21 to E.S.) and by a clinician scientist-program of the Faculty of Medicine of the RWTH Aachen University. PB is supported by the DFG (Project IDs 322900939, 454024652, and 432698239) and the European Research Council (ERC Consolidator Grant No 101001791). E.S. has received a research grant from the German Society of Nephrology (DGfN). VJ is supported by the German Research Foundation SFB/TRR ID 322900939; S-03; (INST 948/4S-1), Cost-Action CA 21165, IZKF Multiorgan complexity in Friedreich Ataxia. IC is supported by the DFG (project GE 2811/3-2) and the E:MED Consortia Fibromap funded by the German Ministry for Science and Education (BMBF). Figure 7 and the graphical abstract were created with BioRender.com.

AUTHOR CONTRIBUTIONS

ES, VJ, and MJM designed research; ES, VJ, TS, VS, ML, and MB performed the research; ES, CM, MB, KL, IVM, CS, PB, CG, TO, and IGC analyzed data; MB and ES designed the figures; MB wrote the article. All authors reviewed and edited the article.

DECLARATION OF INTERESTS

The authors declare no competing interests.

Received: September 2, 2023
Revised: December 5, 2023
Accepted: February 13, 2024
Published: February 16, 2024

REFERENCES

1. Chertow, G.M., Burdick, E., Honour, M., Bonventre, J.V., and Bates, D.W. (2005). Acute kidney injury, mortality, length of stay, and costs in hospitalized patients. J. Am. Soc. Nephrol. *16*, 3365–3370. https://doi.org/10.1681/ASN.2004090740.
2. Ali, T., Khan, I., Simpson, W., Prescott, G., Townend, J., Smith, W., and Macleod, A. (2007). Incidence and outcomes in acute kidney injury: a comprehensive population-based study. J. Am. Soc. Nephrol. *18*, 1292–1298. https://doi.org/10.1681/ASN.2006070756.
3. Li, L., and Xie, T. (2005). Stem cell niche: structure and function. Annu. Rev. Cell Dev. Biol. *21*, 605–631. https://doi.org/10.1146/annurev.cellbio.21.012704.131525.
4. Kurokawa, K., Hayakawa, Y., and Koike, K. (2020). Plasticity of Intestinal Epithelium: Stem Cell Niches and Regulatory Signals. Int. J. Mol. Sci. *22*, 357. https://doi.org/10.3390/ijms22010357.
5. Taub, R. (2004). Liver regeneration: from myth to mechanism. Nat. Rev. Mol. Cell Biol. *5*, 836–847. https://doi.org/10.1038/nrm1489.
6. Tumbar, T., Guasch, G., Greco, V., Blanpain, C., Lowry, W.E., Rendl, M., and Fuchs, E. (2004). Defining the epithelial stem cell niche in skin. Science *303*, 359–363. https://doi.org/10.1126/science.1092436.
7. Hansson, J., Hultenby, K., Cramnert, C., Pontén, F., Jansson, H., Lindgren, D., Axelson, H., and Johansson, M.E. (2014). Evidence for a morphologically distinct and functionally robust cell type in the proximal tubules of human kidney. Hum. Pathol. *45*, 382–393. https://doi.org/10.1016/j.humpath.2013.10.003.
8. Witzgall, R., Brown, D., Schwarz, C., and Bonventre, J.V. (1994). Localization of proliferating cell nuclear antigen, vimentin, c-Fos, and clusterin in the postischemic kidney. Evidence for a heterogenous genetic response among nephron segments, and a large pool of mitotically active and dedifferentiated cells. J. Clin. Invest. *93*, 2175–2188. https://doi.org/10.1172/JCI117214.
9. Smeets, B., Boor, P., Dijkman, H., Sharma, S.V., Jirak, P., Mooren, F., Berger, K., Bornemann, J., Gelman, I.H., Floege, J., et al. (2013). Proximal tubular cells contain a phenotypically distinct, scattered cell population involved in tubular regeneration. J. Pathol. *229*, 645–659. https://doi.org/10.1002/path.4125.
10. Stamellou, E., Leuchtle, K., and Moeller, M.J. (2021). Regenerating tubular epithelial cells of the kidney. Nephrol. Dial. Transplant. *36*, 1968–1975. https://doi.org/10.1093/ndt/gfaa103.
11. Lazzeri, E., Crescioli, C., Ronconi, E., Mazzinghi, B., Sagrinati, C., Netti, G.S., Angelotti, M.L., Parente, E., Ballerini, L., Cosmi, L., et al. (2007). Regenerative potential of embryonic renal multipotent progenitors in acute renal failure. J. Am. Soc. Nephrol. *18*, 3128–3138. https://doi.org/10.1681/ASN.2007020210.
12. Sagrinati, C., Netti, G.S., Mazzinghi, B., Lazzeri, E., Liotta, F., Frosali, F., Ronconi, E., Meini, C., Gacci, M., Squecco, R., et al. (2006). Isolation and characterization of multipotent progenitor cells from the Bowman's capsule of adult human kidneys. J. Am. Soc. Nephrol. *17*, 2443–2456. https://doi.org/10.1681/ASN.2006010089.
13. Berger, K., Bangen, J.M., Hammerich, L., Liedtke, C., Floege, J., Smeets, B., and Moeller, M.J. (2014). Origin of regenerating tubular cells after acute kidney injury. Proc. Natl. Acad. Sci. USA *111*, 1533–1538. https://doi.org/10.1073/pnas.1316177111.
14. Kusaba, T., Lalli, M., Kramann, R., Kobayashi, A., and Humphreys, B.D. (2014). Differentiated kidney epithelial cells repair injured proximal tubule. Proc. Natl. Acad. Sci. USA *111*, 1527–1532. https://doi.org/10.1073/pnas.1310653110.
15. Odutayo, A., Wong, C.X., Farkouh, M., Altman, D.G., Hopewell, S., Emdin, C.A., and Hunn, B.H. (2017). AKI and Long-Term Risk for Cardiovascular Events and Mortality. J. Am. Soc. Nephrol. *28*, 377–387. https://doi.org/10.1681/ASN.2016010105.
16. Coca, S.G., Singanamala, S., and Parikh, C.R. (2012). Chronic kidney disease after acute kidney injury: a systematic review and meta-analysis. Kidney Int. *81*, 442–448. https://doi.org/10.1038/ki.2011.379.
17. Goldstein, S.L., Jaber, B.L., Faubel, S., and Chawla, L.S.; Acute Kidney Injury Advisory Group of American Society of Nephrology (2013). AKI transition of care: a potential opportunity to detect and prevent CKD. Clin. J. Am. Soc. Nephrol. *8*, 476–483. https://doi.org/10.2215/CJN.12101112.
18. Ishani, A., Xue, J.L., Himmelfarb, J., Eggers, P.W., Kimmel, P.L., Molitoris, B.A., and Collins, A.J. (2009). Acute kidney injury increases risk of ESRD among elderly. J. Am. Soc. Nephrol. *20*, 223–228. https://doi.org/10.1681/ASN.2007080837.
19. Kirita, Y., Wu, H., Uchimura, K., Wilson, P.C., and Humphreys, B.D. (2020). Cell profiling of mouse acute kidney injury reveals conserved cellular responses to injury. Proc. Natl. Acad. Sci. USA *117*, 15874–15883. https://doi.org/10.1073/pnas.2005477117.
20. Lou, Q., Hu, Y., Ma, Y., and Dong, Z. (2016). Heat shock factor 1 induces crystallin-αB to protect against cisplatin nephrotoxicity. Am. J. Physiol. Renal Physiol. *311*, F94–F102. https://doi.org/10.1152/ajprenal.00201.2016.
21. Omary, M.B., Ku, N.O., Strnad, P., and Hanada, S. (2009). Toward unraveling the complexity of simple epithelial keratins in human disease. J. Clin. Invest. *119*, 1794–1805. https://doi.org/10.1172/JCI37762.
22. Djudjaj, S., Papasotiriou, M., Bülow, R.D., Wagnerova, A., Lindenmeyer, M.T., Cohen, C.D., Strnad, P., Goumenos, D.S., Floege, J., and Boor, P. (2016). Keratins are novel markers of renal epithelial cell injury. Kidney Int. *89*, 792–808. https://doi.org/10.1016/j.kint.2015.10.015.
23. Rudman-Melnick, V., Adam, M., Potter, A., Chokshi, S.M., Ma, Q., Drake, K.A., Schuh, M.P., Kofron, J.M., Devarajan, P., and Potter, S.S. (2020). Single-Cell Profiling of AKI in a Murine Model Reveals Novel Transcriptional Signatures, Profibrotic Phenotype, and Epithelial-to-Stromal Crosstalk. J. Am. Soc. Nephrol. *31*, 2793–2814. https://doi.org/10.1681/ASN.2020010052.
24. Winyard, P.J., Bao, Q., Hughes, R.C., and Woolf, A.S. (1997). Epithelial galectin-3 during human nephrogenesis and childhood cystic diseases. J. Am. Soc. Nephrol. *8*, 1647–1657. https://doi.org/10.1681/ASN.V8111647.
25. Desmedt, V., Desmedt, S., Delanghe, J.R., Speeckaert, R., and Speeckaert, M.M. (2016). Galectin-3 in Renal Pathology: More Than Just an Innocent Bystander. Am. J. Nephrol. *43*, 305–317. https://doi.org/10.1159/000446376.
26. Numano, F., Inoue, A., Enomoto, M., Shinomiya, K., Okawa, A., and Okabe, S. (2009). Critical involvement of Rho GTPase activity in the efficient transplantation of neural stem cells into the injured spinal cord. Mol. Brain *2*, 37. https://doi.org/10.1186/1756-6606-2-37.
27. Ide, S., Kobayashi, Y., Ide, K., Strausser, S.A., Abe, K., Herbek, S., O'Brien, L.L., Crowley, S.D., Barisoni, L., Tata, A., et al. (2021). Ferroptotic stress promotes the accumulation of pro-inflammatory proximal tubular cells in maladaptive renal repair. Elife *10*, e68603. https://doi.org/10.7554/eLife.68603.
28. Ide, S., Ide, K., Abe, K., Kobayashi, Y., Kitai, H., McKey, J., Strausser, S.A., O'Brien, L.L., Tata, A., Tata, P.R., and Souma, T. (2022). Sex differences in resilience to ferroptosis underlie sexual dimorphism in kidney injury and repair. Cell Rep. *41*, 111610. https://doi.org/10.1016/j.celrep.2022.111610.
29. Liu, J., Kumar, S., Dolzhenko, E., Alvarado, G.F., Guo, J., Lu, C., Chen, Y., Li, M., Dessing, M.C., Parvez, R.K., et al. (2017). Molecular characterization of the transition from acute to chronic kidney injury following ischemia/reperfusion. JCI Insight *2*, e94716. https://doi.org/10.1172/jci.insight.94716.
30. Streuli, C.H. (2009). Integrins and cell-fate determination. J. Cell Sci. *122*, 171–177. https://doi.org/10.1242/jcs.018945.
31. Nony, P.A., and Schnellmann, R.G. (2003). Mechanisms of renal cell repair and regeneration after acute renal failure. J. Pharmacol. Exp. Ther. *304*, 905–912. https://doi.org/10.1124/jpet.102.035022.
32. Abbate, M., Brown, D., and Bonventre, J.V. (1999). Expression of NCAM recapitulates tubulogenic development in kidneys recovering from acute ischemia. Am. J. Physiol. *277*, F454–F463. https://doi.org/10.1152/ajprenal.1999.277.3.F454.
33. Kumar, S., Liu, J., Pang, P., Krautzberger, A.M., Reginensi, A., Akiyama, H., Schedl, A., Humphreys, B.D., and McMahon, A.P. (2015). Sox9 Activation Highlights a Cellular Pathway of Renal Repair in the Acutely Injured Mammalian Kidney. Cell Rep. *12*, 1325–1338. https://doi.org/10.1016/j.celrep.2015.07.034.

34. Kang, H.M., Huang, S., Reidy, K., Han, S.H., Chinga, F., and Susztak, K. (2016). Sox9-Positive Progenitor Cells Play a Key Role in Renal Tubule Epithelial Regeneration in Mice. Cell Rep. *14*, 861–871. https://doi.org/10.1016/j.celrep.2015.12.071.
35. Balzer, M.S., Doke, T., Yang, Y.W., Aldridge, D.L., Hu, H., Mai, H., Mukhi, D., Ma, Z., Shrestha, R., Palmer, M.B., et al. (2022). Single-cell analysis highlights differences in druggable pathways underlying adaptive or fibrotic kidney regeneration. Nat. Commun. *13*, 4018. https://doi.org/10.1038/s41467-022-31772-9.
36. Gerhardt, L.M.S., Liu, J., Koppitch, K., Cippà, P.E., and McMahon, A.P. (2021). Single-nuclear transcriptomics reveals diversity of proximal tubule cell states in a dynamic response to acute kidney injury. Proc. Natl. Acad. Sci. USA *118*, e2026684118. https://doi.org/10.1073/pnas.2026684118.
37. Buse, M., Moeller, M.J., and Stamellou, E. (2022). What We Have Learned so far From Single Cell Sequencing in Acute Kidney Injury. Front. Physiol. *13*, 933677. https://doi.org/10.3389/fphys.2022.933677.
38. Geng, H., Lan, R., Singha, P.K., Gilchrist, A., Weinreb, P.H., Violette, S.M., Weinberg, J.M., Saikumar, P., and Venkatachalam, M.A. (2012). Lysophosphatidic acid increases proximal tubule cell secretion of profibrotic cytokines PDGF-B and CTGF through LPA2- and Gαq-mediated Rho and αvβ6 integrin-dependent activation of TGF-β. Am. J. Pathol. *181*, 1236–1249. https://doi.org/10.1016/j.ajpath.2012.06.035.
39. Wang, Z., and Zhang, C. (2022). From AKI to CKD: Maladaptive Repair and the Underlying Mechanisms. Int. J. Mol. Sci. *23*, 10880. https://doi.org/10.3390/ijms231810880.
40. Zhou, Z., and Zhang, H. (2023). CHAC1 exacerbates LPS-induced ferroptosis and apoptosis in HK-2 cells by promoting oxidative stress. Allergol. Immunopathol. *51*, 99–110. https://doi.org/10.15586/aei.v51i2.760.
41. Zhu, Z.Y., Liu, Y.D., Gong, Y., Jin, W., Topchiy, E., Turdi, S., Gao, Y.F., Culver, B., Wang, S.Y., Ge, W., et al. (2022). Mitochondrial aldehyde dehydrogenase (ALDH2) rescues cardiac contractile dysfunction in an APP/PS1 murine model of Alzheimer's disease via inhibition of ACSL4-dependent ferroptosis. Acta Pharmacol. Sin. *43*, 39–49. https://doi.org/10.1038/s41401-021-00635-2.
42. Wu, D., Hu, Q., Wang, Y., Jin, M., Tao, Z., and Wan, J. (2022). Identification of HMOX1 as a Critical Ferroptosis-Related Gene in Atherosclerosis. Front. Cardiovasc. Med. *9*, 833642. https://doi.org/10.3389/fcvm.2022.833642.
43. Gerhardt, L.M.S., Koppitch, K., van Gestel, J., Guo, J., Cho, S., Wu, H., Kirita, Y., Humphreys, B.D., and McMahon, A.P. (2023). Lineage Tracing and Single-Nucleus Multiomics Reveal Novel Features of Adaptive and Maladaptive Repair after Acute Kidney Injury. J. Am. Soc. Nephrol. *34*, 554–571. https://doi.org/10.1681/ASN.0000000000000057.
44. Myers, B.D., Chui, F., Hilberman, M., and Michaels, A.S. (1979). Transtubular leakage of glomerular filtrate in human acute renal failure. Am. J. Physiol. *237*, F319–F325. https://doi.org/10.1152/ajprenal.1979.237.4.F319.
45. Sutton, T.A. (2009). Alteration of microvascular permeability in acute kidney injury. Microvasc. Res. *77*, 4–7. https://doi.org/10.1016/j.mvr.2008.09.004.
46. Sutton, T.A., Fisher, C.J., and Molitoris, B.A. (2002). Microvascular endothelial injury and dysfunction during ischemic acute renal failure. Kidney Int. *62*, 1539–1549. https://doi.org/10.1046/j.1523-1755.2002.00631.x.
47. Humphreys, B.D., Xu, F., Sabbisetti, V., Grgic, I., Movahedi Naini, S., Wang, N., Chen, G., Xiao, S., Patel, D., Henderson, J.M., et al. (2013). Chronic epithelial kidney injury molecule-1 expression causes murine kidney fibrosis. J. Clin. Invest. *123*, 4023–4035. https://doi.org/10.1172/JCI45361.
48. Yang, L., Brooks, C.R., Xiao, S., Sabbisetti, V., Yeung, M.Y., Hsiao, L.L., Ichimura, T., Kuchroo, V., and Bonventre, J.V. (2015). KIM-1-mediated phagocytosis reduces acute injury to the kidney. J. Clin. Invest. *125*, 1620–1636. https://doi.org/10.1172/JCI75417.
49. McCoy, I.E., Hsu, J.Y., Bonventre, J.V., Parikh, C.R., Go, A.S., Liu, K.D., Ricardo, A.C., Srivastava, A., Cohen, D.L., He, J., et al. (2022). Acute Kidney Injury Associates with Long-Term Increases in Plasma TNFR1, TNFR2, and KIM-1: Findings from the CRIC Study. J. Am. Soc. Nephrol. *33*, 1173–1181. https://doi.org/10.1681/ASN.2021111453.
50. Isaac, J., Tögel, F.E., and Westenfelder, C. (2007). Extent of glomerular tubularization is an indicator of the severity of experimental acute kidney injury in mice. Nephron Exp. Nephrol. *105*, e33–e40. https://doi.org/10.1159/000097017.
51. Hosszu, A., Fekete, A., and Szabo, A.J. (2020). Sex differences in renal ischemia-reperfusion injury. Am. J. Physiol. Renal Physiol. *319*, F149–F154. https://doi.org/10.1152/ajprenal.00099.2020.
52. Appel, D., Kershaw, D.B., Smeets, B., Yuan, G., Fuss, A., Frye, B., Elger, M., Kriz, W., Floege, J., and Moeller, M.J. (2009). Recruitment of podocytes from glomerular parietal epithelial cells. J. Am. Soc. Nephrol. *20*, 333–343. https://doi.org/10.1681/ASN.2008070795.
53. Schönig, K., Schwenk, F., Rajewsky, K., and Bujard, H. (2002). Stringent doxycycline dependent control of CRE recombinase *in vivo*. Nucleic Acids Res. *30*, e134. https://doi.org/10.1093/nar/gnf134.
54. Soriano, P. (1999). Generalized lacZ expression with the ROSA26 Cre reporter strain. Nat. Genet. *21*, 70–71. https://doi.org/10.1038/5007.
55. van Dijk, D., Sharma, R., Nainys, J., Yim, K., Kathail, P., Carr, A.J., Burdziak, C., Moon, K.R., Chaffer, C.L., Pattabiraman, D., et al. (2018). Recovering Gene Interactions from Single-Cell Data Using Data Diffusion. Cell *174*, 716–729.e27. https://doi.org/10.1016/j.cell.2018.05.061.
56. Jankowski, V., Schulz, A., Kretschmer, A., Mischak, H., Boehringer, F., van der Giet, M., Janke, D., Schuchardt, M., Herwig, R., Zidek, W., and Jankowski, J. (2013). The enzymatic activity of the VEGFR2 receptor for the biosynthesis of dinucleoside polyphosphates. J. Mol. Med. *91*, 1095–1107. https://doi.org/10.1007/s00109-013-1036-y.
57. Kork, F., Jankowski, J., Goswami, A., Weis, J., Brook, G., Yamoah, A., Anink, J., Aronica, E., Fritz, S., Huck, C., et al. (2018). Golgin A4 in CSF and granulovacuolar degenerations of patients with Alzheimer disease. Neurology *91*, e1799–e1808. https://doi.org/10.1212/WNL.0000000000006457.

STAR★METHODS

KEY RESOURCES TABLE

REAGENT or RESOURCE	SOURCE	IDENTIFIER
Antibodies		
anti- CD13 AlexaFluor647	Bio-Rad	Cat# MCA2183A647T; RRID:AB_1100678
CD13 Monoclonal Antibody (1C7D7)	Thermofisher	Cat# MA1-181; RRID:AB_2637125
Keratin8/18	Invitrogen	Cat# MA5-32118; RRID:AB_2809410
ANXA2	Sigma Aldrich	Cat# SAB5700074; RRID:AB_2809410
S100A6	Proteintech	Cat# 10245-1-AP; RRID:AB_2183801
S100A10	Thermofisher	Cat# PA527251; RRID:AB_2544727
anti-CD24	BD Biosciences	Cat# 551133; RRID:AB_394064
anti-EGFP	Abcam	Cat# ab13970; RRID:AB_300798
AlexaFluor 594 anti-mouse	Dianova	Cat# 115-585-062; RRID:AB_2338876
AlexaFluor 555 anti-rabbit	Invitrogen	Cat# A27039; RRID:AB_2536100
VCAM	Santa Cruz Biotechnology	Cat# sc-1504; RRID:AB_2214061
Collagen-3	Biotech	Cat# 1330-01; RRID:AB_2794734
Cy2 donkey anti-chicken	Dianova	Cat# 703-225-155; RRID:AB_2340370
Lotus Tetragonolobus Lectin (LTL-FITC)	Vector Laboratories	Cat# FL-1321-2
Chemicals, peptides, and recombinant proteins		
Collagenase type 2	Worthington	LS004174
ProNase	Sigma	P6911;
DNAse	Applichem	A3778
RPMI Medium	ThermoFisher	12633012
7AAD	BD Biosciences	559925
Hoechst 33342	Sigma-Aldrich	SCT118
Single cell 3′ Next GEM V3.1	10x genomics	PN-1000121
Software and algorithms		
CellRanger v3.0.0	10x Genomics	https://support.10xgenomics.com/single-cell-gene-expression/software/pipelines/latest/what-is-cell-ranger
R package Seurat v		https://cran.r-project.org/web/packages/Seurat/index.html
BZ-II analyzing software	Keyence	
GraphPad Prism 9	GraphPad Software	https://www.graphpad.com/scientific-software/prism/
Other		
SONY SH800 sorter	Sony Biotechnology	
MALDI-TOF mass spectrometer Rapiflex™	Bruker Daltonics	
10x Chromium Controller	10x Genomics	Cat.# 1000202
70µm Cell strainer	Miltenyi	130-098-462
4070µm Cell strainer	Miltenyi	130-098-458
Keyence BZ-9000 microscope	Keyence	https://www.keyence.de/products/microscope/fluorescence-microscope/bz-9000/models/bz-9000e/
Microaneurysm clamp	Roboz	RS-5424
Data-availability		https://ncbi.nlm.nih.gov/geo/query/acc.cgi?acc=GSE207020

RESOURCE AVAILABILITY

Lead contact

Further information and requests for resources and reagents should be directed to and will be fulfilled by the lead contact Eleni Stamellou (stamellou.eleni@gmail.com).

Materials availability

This study did not generate new unique reagents.

Data and code availability

- Single-cell RNA-seq data have been deposited at GEO and are publicly available as of the date of publication at the following link. The accession number is listed in the key resources table. https://www.ncbi.nlm.nih.gov/geo/query/acc.cgi?acc=GSE207020.

All of the package version information is here: https://github.com/CostaLab/kidney_injury_lineage/blob/main/requirements.txt.

- The source code has been deposited to GitHub: https://github.com/CostaLab/kidney_injury_lineage.
- Any additional data or information required to reanalyze the data reported in this paper in available from the lead contact upon request.

EXPERIMENTAL MODEL AND STURDY PARTICIPANT DETAILS

Human-samples: Ethics statement

The local ethics committee of the University Hospital RWTH Aachen approved human tissue protocols (EK-No. 042-17). All patients provided informed consent and the study was performed in accordance with the Declaration of Helsinki. All human samples were collected as part of the Care for Home study at the outpatient clinic of the Saarland University Medical Center and was additionally approved by the Saarland University Ethics Committee. In this study the patients were from Europe and white. The ethnicity and socioeconomic status were not part of the study.

More detailed information about the participants can be found in Table 2.

Animal studies - Mice

- All animal experiments were approved by the Landesamt für Natur, Umwelt und Verbraucherschutz Nordrhein-Westfalen.
- The transgenic PEC-rtTA mouse has been described previously.[6,52–54]
- All mice were 9 weeks old and male.
- Mice were housed at two to five mice per cage with a 12-h light–dark cycle at sustained temperature (20°C ± 0.5°C) and humidity (approximately 50% ± 10%) with *ad libitum* access to food and water. Doxycycline was administrated once as i.p injection (50 μg/g body weight dissolved in 0.45% saline) immediately after induction of the ischemic injury and for the 4 weeks model 24 hours before euthanasia.
- Ischemia reperfusion injury model: All surgeries were performed by the same investigator. Mice were anesthetized with ketamine–xylazine (100 mg/ml ketanest and 20 mg/ml xylazine in normal saline 0.9%; 0.1 ml per 10 g of body weight). Kidneys were exposed via dorsal incision. Renal pedicle of left kidney was exposed and clamping was performed with arterial clip for 35 minutes. After this time, the clip was removed and the kidney was reperfused. The cut was sutured and the mice were monitored after surgery and received analgesia (Buprenorphin 0.1mg/kg s.c). Animals were sacrificed and blood and kidneys were sampled 8, 24 and 48 hours and 6, 12 and 28 days post-ischemia.

Lineage-tracing

The PEC-rtTA/LC1/R26R is based on two reporter genes (*LacZ and H2B-eGFP*). Under the control of a promoter from parietal epithelial cells (PEC-promoter) and Doxycycline, both reporter genes are expressed.

The promoter used in the PEC/rtTA system is a chimeric construct that combines elements from different species (human and rabbit podocalyxin) and is therefore not a native sequence of the murine genome (https://www.informatics.jax.org/allele/MGI:6400996). As such, the cis and trans factors governing a murine promoter remain unknown.[52]

Under the control of the PEC-promoter, a transactivator is expressed. This transactivator is doxycycline-dependent. Therefore, when doxycycline is administered, the transactivator binds along with doxycycline to transactivator-dependent promoters. In the mouse line, two transactivator-dependent promoters exist:

1. *LacZ* (corresponding protein: *β*-Galactosidase): The transactivator, along with Doxycycline, binds to a transactivator-responsive element (TRE). This activates a Cre-recombinase that cuts out a stop codon (flanked by two loxP sites). Since this stop codon cannot be reinserted later, this step is **irreversible**. As a result, the cells permanently express the *LacZ* (provided that they have adopted the regenerative STC phenotype at some point and received Doxycycline). The expression of *LacZ* is controlled by the Rosa26 locus

(a ubiquitously active gene locus). By administering a dye, the B-Galactosidase enzyme can process this dye, allowing the cells to be stained in the cytoplasm.

2. *H2B-eGFP*: To express the other reporter gene (*H2B-eGFP*), the transactivator binds along with doxycycline to a transactivator-responsive element. This leads to the expression of *H2B-eGFP*. However, the *H2B-eGFP* reporter gene is **not** irreversibly expressed after activation of the STC phenotype. Once the cells downregulate the STC program, *H2B-eGFP* is reduced/no longer expressed. However, since the protein was initially expressed, it remains in the cell nucleus (bound to histones) until it is eventually degraded.

METHOD DETAILS

Mouse kidney samples

Mice were euthanized with isoflurane, blood was collected, and the left ventricle was perfused with 20 ml NaCl 0.9% to remove residual blood from the vasculature. Kidneys from 3 mice to average out the individual variabilities at each time point were harvested at hour 8 and day 1, 2, 6, 12, and 28 after the unilateral ischemia-reperfusion injury for scRNA-seq and histologic verification. Contralateral kidneys from day 2 were harvested as well for scRNA-seq and histologic verification. Validations were performed on an additional set of animals treated with the identical unilateral ischemia-reperfusion injury procedure (n=3 per group).

Isolation of single cells

The kidneys were placed on ice-cold Dulbecco's phosphate-buffered saline, decapsulated, and bisected lengthwise. The cortical regions were then finely minced with a sterile scalpel until tissue was homogenous. Next, the minced tissue was placed in 5ml digestion buffer containing 21.4 mg/ml collagenase type 2 (Worthington), 7.1 mg/ml ProNase E (P6911; Sigma), 5 U/ml DNAse (A3778; Applichem) made up in RPMI medium. The digest mix was incubated in a 37°C water bath for 20 minutes with vigorous trituration with a 1 ml pipet every 5 minutes. After 20 minutes, the digest mix was subsequently added to a 70-μm filter (130-098-462; Miltenyi) on a 50-ml conical tube. The filter was rinsed with 20 ml RPMI medium and the flow through was then added to a 30-μm filter (130-098-458; Miltenyi) on a 50-ml conical tube. The filter was rinsed again with 20 ml RPMI medium. Next, the cells were pelleted by centrifugation at 350 × g for 5 minutes at 4°C. The supernatant was discarded, and the pellet resuspended in 1 ml 1% fetal bovine serum (FBS) in PBS.

FACS

Cells were labelled with following antibodies: anti-CD13 (Rat Anti-Mouse CD13 AlexaFluor647, RRID: AB_1100671, Bio-Rad, Düsseldorf, Germany) and 7AAD (BD Biosciences, Allschwil, Switzerland). Isolated cells were resuspended in 1% FBS in PBS on ice. The cells were sorted in the semi-purity mode with the SONY SH800 sorter (Sony Biotechnology; 100-μm nozzle sorting chip Sony). Finally, cells were analyzed with a hemocytometer using trypan blue. Overall, the viability was more than 80% using this method.

Tubular injury score

Tubular injury score was assessed by PAS staining and determined using a semiquantitative scoring system in 15 fields for each specimen at 20x magnification. The score included: atypical cytoplasmic vacuolization, tubular necrosis, tubular dilatation, cell detachment, loss of brush border and denuded basement membrane. Using these parameters, the scale of injury was from 1 to 5; score 1: no abnormality; score 2: lesions affecting <10% of kidney sample; score 3: lesions affecting 10% to 25% of kidney sample; score 4: lesions affecting 26% to 50% of kidney sample; and score 5: lesions affecting >75% of the kidney sample.

Light microscopy

For light microscopy, the 4% buffered formalin-fixed kidney fragments were dehydrated and embedded in paraffin. The 4-μm paraffin sections were stained with PAS.

Serum creatinine measurement

Levels of serum creatinine were analyzed using a Hitachi 9-17-E autoanalyzer (Hitachi, Frankfurt am Main, Germany).

Immunofluorescence staining

Immunofluorescence staining was performed on 2-μm paraffin-embedded sections. Antibodies included the following: KRT8/18 (Cat. No: MA5-32118, Invitrogen, Massachusetts, USA), LGALS3 (Cat. No:14979-1-AP, Proteintech, Planegg, Germany), ANXA2 (Cat. No: SAB5700074, Sigma Aldrich, St. Louis, MO), S100A6 (RRID: AB_2183801, Proteintech, Planegg, Germany), S100A10 (PA5-95505, Thermofisher, Karlsruhe, Germany), CD24 (RRID: AB_1727452, BD Biosciences, San Jose California, USA), EGFP (RRID: AB_2936447, Abcam, Cambridge, UK), KIM-1 (Cat. No:LS-B6567, LS Bio,Washington,USA), VCAM-1(RRID: AB_2214061, Cat. No: sc-1504, Santa Cruz, Texas, USA), Sox-9 (H Cat. No: PA001759, Sigma Aldrich, St. Louis, MO). Immunostaining was performed as described previously.[13] The following secondary antibodies were used: AlexaFluor 594 anti-mouse (Dianova, Hamburg Germany), AlexaFluor 555 anti-rabbit (Invitrogen, Carlsbad, USA), Cy2 donkey anti-chicken (Dianova, Hamburg, Germany). The nuclei were stained using Hoechst 33342 (Sigma-Aldrich, St. Louis, MO). Sections were evaluated with a Keyence BZ-9000 microscope using BZ-II analyzing software (Keyence Corporation, Osaka, Japan). Analysis of

distributions of enhanced green fluorescent protein (eGFP) on PTs was performed on sections counterstained with Hoechst and Fluorescein-labeled Lotus Tetragonolobus Lectin (LTL-FITC; Vector Laboratories, Burlingame, CA).

CD13-quantification

A section from each animal was stained with CD13 and DAPI in immunofluorescence. Four representative images were taken per section. Thus, from three biopsies, we obtained 12 images per time point. The number of DAPI-positive cells was evaluated semi-automatically, while CD13-positive cells were evaluated manually.

Collagen-3-quantification

A section from each animal was stained with Collagen-3 in Immunhistochemistry. Three biopsies were used at each time point and twelve representative images were examined from each biopsy. The collagen-3 positive area was quantified using ImageJ.

Immunhistochemistry

Immunofluorescence staining was performed on 2-μm paraffin-embedded sections. Antibodies included the following: Collagen-3 (RRID: AB_2214061, Cat. No: sc-1504, Santa Cruz, Texas, USA). Sections were evaluated with a Keyence BZ-9000 microscope using BZ-II analyzing software (Keyence Corporation, Osaka, Japan). Analysis of the Collagen-3 expression was quantified using ImageJ. Three biopsies were used at each time point (12 days and 4 weeks after AKI). Twelve representative images were examined from each biopsy. An individual threshold was set for each image.

scRNA-seq data analysis

We preprocessed the scRNA sequencing data with cellranger pipeline (3.1.0) for each library. Next, we used Seurat (V4.0.1.) for downstream analysis. First, we created a Seurat object from count matrices. Next, we used threshold 50% of mitochondrial fraction to remove bad quality cells (Figure S6A). Next, we filtered the data by only retaining cells with RNA expressed in more than 400 cells and UMI counts in less than 40,000 (Figure S6B). Next, we call CellCycleScoring to obtain the Sscore and G2M score. Then, we normalized the data followed by regressing out cell cycle and mitochondrial content by calling ScaleData. scRNA-seq matrices from distinct conditions were integrated by the functions FindIntegrationAnchors and IntegrateData. We ran PCA (20 PCs) to reduce the dimensionality and used UMAP to visualize the data. To annotate the population, we first called FindNeighbors and FindClusters to obtain the clusters (resolution of 0.5). Next, we ran FindAllMarkers to find gene markers for each cluster (p-value < 0.05), with which we are able to annotate these clusters with curated marker genes. We performed another filtering by only retaining PTs for the analysis. For the pathway analysis, we performed GO, Reactome and hallmark with R package ClusterProfiler (version 4.0.5). We used ArchR(1.0.1) to fit trajectories. First, we ran DiffusionMap with the destiny package (version 3.9.0), next we performed clustering on the diffusion embeddings and constructed trajectories with the clusters. For gene expression plots, we utilized the Rmagic package to impute the gene score.[55] We applied the same filtering threshold, integration and clustering for the sequenced data STCs 4 weeks after AKI.

Mass spectrometry of serum proteins (MALDI MS)

30 μg protein was separated by SDS-polyacrylamide gel electrophoresis. Proteins were stained using Coomassie Brilliant Blue G-250 (BioRad, Munich, Germany). The Gel plugs were separated and the resulting plugs were washed and equilibrated using ammonium bicarbonate in acetonitrile. The isolated protein was digested by trypsin and analyzed by matrix-assisted-laser-desorption/ionization-time-of-flight-mass spectrometry (MALDI-TOF-TOF) as previously described.[56] Briefly, the protein plugs were incubated with ammonium bicarbonate (50 mmol l^{-1}) and 0.03% w/c trypsin for 24h at 37°C. The resulting tryptic peptides were desalted and concentrated by using $ZipTip_{c18}$ technology (Millipore, Billerica, MA, USA) and eluted with 80% acetonitrile directly onto the (MALDI) target plate (MTP-Ground steel 400/384; Bruker-Daltonic, Germany) using alpha-cyano-4-hydroxycinnamic acid as matrix. The subsequent mass-spectrometric (MS) analyses were performed using a MALDI-time of flight/time of flight (TOF/TOF) mass spectrometer (Ultraflex III; Bruker-Daltonic, Germany) and a Rapiflex MS , Bruker-Daltronic, Germany). The MALDI-TOF/TOF instrument was equipped with a smart-beam laser operated at a 100–200 Hz repetition rate. The presented spectra are the representative average spectra with sum of 200 single-shot spectra for MS mode. The positively charged ions mass-spectra were analysed in the reflector mode using delayed ion-extraction. The MALDI-Orbitrap instrument was equipped with a nitrogen laser (MNL-100; LTB Lasertechnnik, Germany) operating at a wavelength of 337.1nm with a spectral bandwidth of 0.1nm, pulse repetition rate up to 60 Hz with 3ns pulse width and 75μJ energy per pulse. Fourier-transform mass-spectrometric (FTMS) data were acquired in a measuring grid across the membrane area with a resolution of 60,000 in a positive range.

Mass spectrometry of serum proteins (MALDI MS)

The CARE FOR HOME study comprises stable patients with confirmed CKD recruited at the outpatient clinic of the Saarland University Medical Center. All patients in this study were from Europe and white. The ethnicity and socioeconomic status were not collected. The study was approved by the Saarland University Ethics Committee and all participants gave their written consent.

A total of 15 measurements were performed on 5 healthy controls, 5 chronic kidney disease (CKD) stage 2 patients, and 5 CKD stage 3 patients. Plasma was prepared as described before[57] and a MALDI–time of flight (TOF)/TOF MS (Ultraflex III; Bruker Daltonic, Bremen,

Germany) MS was performed. A database search (Swiss-Prot) using the Mascot 2.2 search engine (Matrix Science Inc, Boston, MA) and Bruker Bio-Tool 3.2 software was performed with the calibrated and annotated spectra to calculate the peptide mass signal for each entry into the sequence database, to compare the experimental MALDI-MS and MALDI-MS/MS dataset, and to assign a statistical weight to each individual peptide match using empirically determined factors.[56]

QUANTIFICATION AND STATISTICAL ANALYSES

Data are presented as mean ± SD if not specified otherwise. Comparison of two groups was performed using unpaired *t*-test. If data were not normally distributed wilcoxon rank sum test was used. For multiple group comparison, one-way ANOVA with Bonferroni's multiple comparison test was applied. Statistical analyses were performed using GraphPad Prism 8 (GraphPad Software). $P < 0.05$ was considered significant. For marker findings we used default Wilcoxon test for Seurat. For PROGENy comparison, we also used the Wilcoxon test. *** when p-value < 0.001, ** when p-value <0.01, * when p-value<0.01, ns otherwise. All statistical results could be found in the figures or legends. Three biological replicates (n = 3) were used unless otherwise indicated in the text or figure caption. Statistical tests were performed using GraphPad.